Author Manuscript

Author Manuscript

Author Manuscript

Author Manuscript

HHS Public Access

Author manuscript

Alcohol Clin Exp Res. Author manuscript; available in PMC 2017 December 01.

Published in final edited form as:

Alcohol Clin Exp Res. 2016 December ; 40(12): 2573–2590. doi:10.1111/acer.13247.

Study of ethanol-induced Golgi disorganization reveals the potential mechanism of alcohol-impaired N-glycosylation

Carol A. Casey[1], **Ganapati Bhat**[2], **Melissa S. Holzapfel**[3], and **Armen Petrosyan**[2,*]

[1]Department of Internal Medicine, University of Nebraska Medical Center, and the Fred and Pamela Buffett Cancer Center, Omaha, NE, USA

[2]Department of Biochemistry and Molecular Biology, College of Medicine, University of Nebraska Medical Center, and the Fred and Pamela Buffett Cancer Center, Omaha, NE, USA

[3]Department of Pathology and Microbiology, University of Nebraska Medical Center, and the Fred and Pamela Buffett Cancer Center, Omaha, NE, USA

Abstract

Background—It is known that ethanol (EtOH) and its metabolites have a negative effect on protein glycosylation. The fragmentation of the Golgi apparatus induced by alteration of the structure of largest Golgi matrix protein, giantin, is the major consequence of damaging effects of EtOH-metabolism on the Golgi, however, the link between this and abnormal glycosylation remains unknown. Because previously we have shown that Golgi morphology dictates glycosylation, we examined the effect EtOH administration has on function of Golgi residential enzymes involved in N-glycosylation.

Methods—HepG2 cells transfected with mouse ADH1 (VA-13 cells) were treated with 35 mM ethanol for 72 h. Male Wistar rats were pair-fed Lieber-DeCarli diets for 5 to 8 weeks. Characterization of Golgi-associated mannosyl (α-1,3-)-glycoprotein beta-1,2-N-acetylglucosaminyltransferase (MGAT1), α-1,2-mannosidase (Man-I) and α-mannosidase II (Man-II) were performed in VA-13 cells and rat hepatocytes followed by 3D Structured Illumination Microscopy (SIM).

Results—First, we detected that EtOH administration results in the loss of sialylated N-glycans on asialoglycoprotein receptor, however the high mannose-type N-glycans are increased. Further analysis by 3D SIM microscopy revealed that EtOH treatment despite Golgi disorganization does not change *cis*-Golgi localization for Man-I, but does induce *medial*-to-*cis* relocation of MGAT1 and Man-II. Using different approaches, including electron microscopy, we revealed that EtOH treatment results in dysfunction of Arf1 GTPase followed by a deficiency in COPI vesicles at the Golgi. Silencing beta-COP or expression of GDP-bound mutant Arf1(T31N) mimics the EtOH effect on retaining MGAT1 and Man-II at the *cis*-Golgi, suggesting that (a) EtOH specifically blocks activation of Arf1, and (b) EtOH alters the proper localization of Golgi enzymes through

*Address correspondence to: Armen Petrosyan, Department of Biochemistry and Molecular Biology, University of Nebraska Medical Center, Omaha, NE 68198-5870. Tel: +1402 559-7718; Fax: +1402 559-6650; apetrosyan@unmc.edu.

Competing financial interests

The authors declare no competing financial interests.

Author Manuscript Author Manuscript Author Manuscript Author Manuscript

impairment of COPI. Importantly, the level of MGAT1 was reduced, because likely MGAT1, contrary to Man-I and Man-II, is giantin-sensitive.

Conclusions—Thus, we provide the mechanism by which EtOH-induced Golgi remodeling may significantly modify formation of N-glycans.

Keywords

Ethanol; Golgi fragmentation; abnormal N-glycosylation; COPI

INTRODUCTION

Chronic alcohol abuse and alcoholism are known to cause alcoholic liver disease (ALD), which remains a major cause of liver-related mortality in the US and worldwide (NIAAA, 2014). The negative effect of ethanol (EtOH) and its metabolites on protein glycosylation has been well studied. For example, the activities of a dolichyl-phosphate β-D-mannosyltransferase in the endoplasmic reticulum (ER), and galactosyltransferase and sialyltransferase in the Golgi are reduced after EtOH treatment (Guasch et al., 1992; Cottalasso et al., 1996). In addition, chronic alcohol administration results in the accumulation of glycoproteins that carry non-reduced mannose (Braza-Boils et al., 2006). Moreover, several independent studies indicate the presence of intermediate or truncated forms of N-linked glycans on glycoproteins in patients with chronic alcohol abuse, including carbohydrate-deficient transferrin (Gravel et al., 1996; Waszkiewicz et al., 2012). Methylpyrazole, an inhibitor of alcohol dehydrogenase (ADH), when administrated *in vivo* prevents the EtOH-induced inactivation of glycosyltransferases, suggesting that impairment of glycosylation in the liver is primarily mediated by products of the oxidative metabolism of EtOH (Marinari et al., 1993). However, in spite of our increasingly detailed molecular understanding, important and as-yet unanswered questions remain concerning the machinery of alcohol-induced abnormal glycosylation.

It is known that EtOH administration alters the structure of the Golgi apparatus, the central station of glycosylation (Renau-Piqueras et al., 1987; Zimmerman, 1999). We have recently shown that ADH-catalyzed oxidation of EtOH is a major contributor of alcohol-induced Golgi fragmentation, and that this is initiated by downregulation of SAR1A GTPase, an essential component of COPII vesicles (Petrosyan et al., 2015a). We have found that COPII vesicles are required for Golgi delivery of the protein disulfide isomerase A3 (PDIA3), an enzyme that catalyzes dimerization of the largest Golgi matrix protein, giantin. Giantin is necessary for maintaining Golgi structure (Koreishi et al., 2013; Asante et al., 2013; Petrosyan et al., 2014), which is normally composed of the parallel series of flattened, disk-shaped cisternae. EtOH treatment impairs formation of COPII, thus blocking Golgi targeting for PDIA3 and subsequent dimerization of giantin, which, in turn, causes Golgi disorganization. In addition to COPII, COPI vesicles appeared to be affected by EtOH (Ktistakis et al., 1996); however the details and functional consequences of EtOH-induced impairment of COPI have never been studied.

The role for COPI vesicles and its mechanisms of secretory transport through the Golgi is still a subject of much debate in the Golgi research community. According to the classical

Author Manuscript Author Manuscript Author Manuscript Author Manuscript

vesicular model, Golgi cisternae are stable compartments, and the anterograde movement of cargo is carried by COPI that moves from the proximal cisterna to the adjacent, distant one. In this scenario, the localization of Golgi enzymes appears to be stationary according to the order in which the enzymes function (Orci et al., 1997). The alternative view is the cisternal maturation model, which postulates that Golgi is dynamic, because cisternae move from the pre-Golgi intermediates to the trans-Golgi network, and newly formed membranes gradually replace older membranes (Mironov et al., 1997). This conception holds that COPI vesicles provide retrograde (from *trans* to *cis*) intra-Golgi transportation of Golgi resident proteins, thereby achieving their differential Golgi localization. Indeed, several independent groups detected the concentration of Golgi enzymes, for example α-mannosidase II (Man-II), in COPI vesicles (Lanoix et al., 2001; Martinez-Menarguez et al., 2001). Moreover, all three enzymes studied here, α-1,2-mannosidase (Man-I), Man-II, and mannosyl (α-1,3-)-glycoprotein beta-1,2-N-acetylglucosaminyltransferase (MGAT1), have been found in COPI vesicles in concentrations higher than those in Golgi membranes, according to a quantitative proteomics map of the ER and Golgi fractions isolated from rat liver homogenates (Gilchrist et al., 2006). Notably, Rothman and coauthors (Orci et al., 2000) assumed that COPI may carry Golgi enzymes in intra-Golgi “straightforward fashion”, however this prediction was not experimentally proved. Also, we are still far from having a complete understanding of whether link exists between perturbations in Golgi morphology and reordering of Golgi enzymes and subsequent alteration in N-/O-glycosylation. While several observations, including our own, indicate that different cases of Golgi fragmentation are accompanied by selective downregulation of glycosyltransferases (Kellokumpu et al., 2002; Pokrovskaya et al., 2011; Petrosyan and Cheng, 2014; Petrosyan et al., 2014; Petrosyan, 2015), the details and related mechanisms are still poorly understood.

Here, the comprehensive analysis of the N-glycans on the hepatic asialoglycoprotein receptor (ASGP-R) from EtOH-treated specimens revealed a decrease of complex-type N-glycans, coupled with an increase of $Man_5GlcNAc_2$-dominated high-mannose-type N-glycans. We next took advantage of superresolution microscopy to study whether EtOH-induced Golgi fragmentation alters trafficking of the Golgi enzymes involved in the initial step of N-glycosylation. We found that EtOH specifically alters Golgi delivery for MGAT1 and induces re-compartmentalization of MGAT1 and Man-II. Of note, the depletion of giantin reduces the level of MGAT1 in the Golgi, implying that altered N-glycosylation is likely to be an indirect consequence of deficiency in giantin. Finally, we observed that EtOH abolishes COPI vesicles at the Golgi, and that the effect EtOH has on reordering of Golgi enzymes can be reproduced by silencing β-COP or overexpression of mutant Arf1. Thus, our study provides the potential mechanism of EtOH-related abnormal glycosylation.

MATERIALS AND METHODS

Antibodies and reagents

The primary antibodies used were: a) rabbit polyclonal – giantin (ab24586), ASGP-R1 (ab88042) , Man-II (ab12277), Ubiquitin (ab7780) and Calreticulin (ab4) (Abcam); b) rabbit monoclonal – Man-I (ab140613), MGAT1 (ab180578), GM130 (ab52649) (Abcam); c) mouse monoclonal – GRASP65 (sc365434, Santa Cruz Biotechnology), β-actin (A2228,

Author Manuscript Author Manuscript Author Manuscript Author Manuscript

Sigma), giantin (ab37266), β-COP (ab6323) and MRP2 (ab3373) (Abcam); d) mouse polyclonal – MGAT1 (ab167365), GM130 (ab169276) (Abcam). The secondary antibodies (Jackson ImmunoResearch) were: a) HRP-conjugated donkey anti-rabbit (711-035-152) and donkey anti-mouse (715-035-151) for Western-blotting; b) donkey anti-mouse Alexa Fluor 488 (715-545-150) and anti-rabbit Alexa Fluor 594 (711-585-152) for immunofluorescence. F-actin staining was performed using CytoPainter F-actin Staining Kit-Blue Fluorescence according to the manufacture's (Abcam) protocol. Peptide N-glycosidase F (PNGase F) was purchased from NEB, UK (P0704S). Graphite columns were procured by Thermo Scientific, USA (88302). MG-132 (474790) was obtained from EMD Chemicals (Brookfield, WI). All other chemicals and reagents used, such as acetonitrile, EtOH, methanol, sodium hydroxide, methyl iodide, and DMSO were of MS-grade/analytical grade and purchased from Sigma.

Cell culture, EtOH administration, polarization of VA-13 cells, isolation of hepatocytes, and transfection

HepG2 cells transfected with mouse ADH1 (VA-13 cells) were obtained from Dr. Dahn Clemens at the Department of Veterans Affairs, Nebraska Western Iowa HCS (Clemens et al., 2002). VA-13 cells were grown in Dulbecco's modified Eagle medium (DMEM) with 4.5g/ml glucose, 10% FBS, non-essential amino acids and 100U/ml of Penicilin +Streptomycin. Twenty-four hours after seeding cells (at ~75% confluence), culture media were changed for one containing 35 mM EtOH for another 72 h. The medium was replaced every 12 h to maintain a constant EtOH concentration. Control cells were seeded at the same time as treated cells and maintained on the same medium; EtOH was replaced by the appropriate volume of medium to maintain similar caloric content.

For analysis of VA-13 cells polarization, cells were stained for apical multidrug-resistant protein 2 (MRP2) and F-actin. Cell nuclei were visualized using DAPI (Invitrogen). The polarity index was determined by counting the number of F-actin- and MRP2-positive apical structures per 100 nuclei using the Zeiss LSM 800 Confocal Laser Microscope with the Airyscan module as previously reported (Mee et al., 2009).

Primary rat hepatocytes from control and EtOH-fed animals were prepared from male Wistar rats. Rats weighing 140-160 g were purchased from Charles River Laboratories. Initially, the animals were fed a Purina chow diet and allowed to acclimate to their surroundings for a period of 3 days. Then the rats were paired according to weight and fed either control or EtOH containing (35% fat, 18% protein, 11% carbohydrates, 36% EtOH) Lieber-DeCarli diet for periods of 5-7 weeks (Dyets, Inc). The control diet was identical to the ethanol diet except for the isocaloric substitution of ethanol with carbohydrates (Lieber and DeCarli, 1982). This protocol was approved by the Institutional Animal Care and Use Committee of the Department of Veterans Affairs, Nebraska Western Iowa HCS, and the University of Nebraska Medical Center.

Hepatocytes were obtained from the livers of control and ethanol-fed rats by a modified collagenase perfusion technique as described and used previously by the Casey laboratory (Casey et al., 1987; Tworek et al., 1996). The primary hepatocytes isolated from control and ethanol treated animals were cultured as previously described (Schaffert et al., 2001). Briefly, freshly isolated hepatocytes were seeded in William's media on collagen coated 6

Author Manuscript Author Manuscript Author Manuscript Author Manuscript

well plates with or without coverslips. After 2 hours in culture, cells were washed with PBS, followed by incubation with 5% FBS-Williams media. Cells were maintained at 37°C in 5% CO2 for the indicated time. Additional cell aliquots were washed in cold phosphate-buffered saline, and the pellets were stored at −70°C for future analysis.

The active, GTP bound form of Arf1 was detected by Arf1Activation Assay Kit (Cell Biolabs). Briefly, this kit utilizes GGA3 PBD Agarose beads to selectively isolate and pull-down the active form of Arf from purified samples or endogenous lysates. Subsequently, the precipitated GTP-Arf is detected by Western blot analysis using an anti-Arf1 antibody. *COPB* (β-COP), *MGAT1*, *GOLGB1* (giantin), *GOLGA2* (GM130) and scrambled on-targetplus smartpool siRNAs were purchased from Santa Cruz Biotechnology. All products were consisted of pools of three target-specific siRNAs. Cells were transfected with *COPB* (100 nM for 72 h), *MGAT1* (50 nM for 72 h), *GOLGB1* (100 nM for 72 h), *GOLGA2* (100 nM for 72 h) siRNAs using Lipofectamine RNAi MAX reagent (Life science technologies). Arf1(T31N)-EGFP was a gift from Marci Scidmore (Addgene plasmid # 49580). Transient transfection of VA-13 cells was carried out using the Lipofectamine 2000 (Life Science technologies) following the manufacturer's protocol.

Confocal immunofluorescence microscopy

Staining of cells and tissue sections was performed by the methods described previously (Petrosyan and Cheng, 2013). Slides were examined under a LSM 800 Zeiss Airyscan microscope performed at the Advanced Microscopy Core Facility of the University of Nebraska Medical Center. Images were analyzed using ZEN 2009 software. For some figures, image analysis was performed using Adobe Photoshop and ImageJ.

Three-dimensional structured illumination (3D-SIM) microscopy and image analysis

SIM imaging of Golgi ribbons was performed on a Zeiss ELYRA PS.1 superresolution scope (Carl Zeiss Microscopy, Germany) using an PCO.Edge 5.5 camera equipped with a Plan-Apochromat 63×1.4 oil objective. Optimal grid sizes for each wavelength were chosen according to the recommendations of the manufacturer. For 3D-SIM, stacks with a step size of 110 nm were acquired sequentially for each fluorophore, and each fluorescent channel was imaged with three pattern rotations with 3 translational shifts. The final SIM image was created using modules build into the Zen Black software suite that accompanies the imaging setup. Analyses were undertaken on 3D-SIM data sets in 3D using IMARIS versions 7.2.2–7.6.0 (Bitplane Scientific). The 3D mask was obtained by applying a Gaussian filter to merged channels, thresholding to remove low-intensity signals, and converting the obtained stack into a binary file that mapped all voxels of interest for coefficient calculation. For colocalization studies, IMARIS 'Colocalization Module' was used. To avoid subjectivity, all thresholds were automatically determined using algorithms, based on the exclusion of intensity pairs that exhibit no correlation (Costes et al., 2004). Colocalization was determined by Pearson's coefficient. The average of maximum of inter-fluorescence label distance was calculated as follows: using a scale bar, we first determined the measured unit value, corresponding to 1 μm, on each 3D SIM micrographs that we used. Then, using the line tool in ImageJ, we obtained unit value from 10 to 12 different Golgi regions for

Author Manuscript Author Manuscript Author Manuscript Author Manuscript

conversion into micromillimeter scale. The average from the different number of cells were presented as mean ± SD.

Isolation of Golgi membrane fractions by sucrose gradient flotation

Golgi membrane fractions were isolated using methods described previously (Petrosyan and Cheng, 2013).

Mass spectrometric analysis of N-glycans

ASGP-R in cell lysate was subjected to IP (Thermo Scientific) with ASGP-R1 Ab, followed by separation on 15% SDS-PAGE and stained by Coomassie Blue. The gel slice containing ASGP-R was destained and dehydrated with acetonitrile (Shevchenko et al., 2006), followed by incubation with Peptide N-glycosidase F (PNGase F, 150 U/ml) at 37 °C for 16 h. The glycans were extracted from the gel with 200 μl of 50% acetonitrile by sonication for 1h, subsequently twice followed by water. Then, all the fractions were pooled and dried under vacuum (Sagi et al., 2005). Extracted N-glycans were purified using non porous graphite columns (Thermo scientific) followed by permethylation using DMSO and sodium hydroxide in the presence of methyl iodide as described by Morelle and Michalski, 2007. MALDI-TOF data were obtained using a 4800 MALDI-TOF/TOF mass spectrometer (AB Sciex USA Ltd.) in the positive reflector ion mode. The data were obtained using 4000 series explorer software, and analyzed using Expasy database online and also by the Consortium for functional glycomics (CFG) database. Structural assignments were made based on MALDI mass and confirmed by ms/ms fragmentation.

Transmission Electron Microscopy

EM was performed using protocols described previously (Petrosyan et al., 2014).

RESULTS

Polarization of VA-13 cells is dispensable for EtOH-induced Golgi fragmentation

In an effort to identify the mechanism of abnormal glycosylation of proteins in EtOH-treated hepatocytes, we employed human hepatoma HepG2 cells, which is considered an appropriate cell culture model system to study the apical plasma membrane biogenesis, i.e., the development of cell polarity (Bouma et al., 1989; Chiu et al., 1990; Sormunen et al., 1993; Zaal et al., 1994; Zegers et al., 1998). While HepG2 cells are capable of displaying formation of apical and basolateral cell surface domains (van IJzendoorn et al., 1997, 2004) that resemble the bile canalicular (BC) and sinusoidal domains, respectively, only 20-40% of cells are polarized (Theard et al., 2007). Previously, we have shown that in VA-13 cells (HepG2 cells transfected with mouse ADH1) Golgi undergoes significant disorganization in response to EtOH treatment (Petrosyan et al., 2015a, 2016). Because during cell polarization Golgi shows reorientation to the apical-most region close to the minus ends of the vertical microtubules (Bacallao et al., 1989), we were interested whether the link exists between EtOH-induced Golgi fragmentation and cells polarization. We visualized the appearance of the apical lumen (BC) by the presence of two markers: F-actin, which is widely presented underneath the apical surface (Zegers and Hoekstra, 1997), and MRP2, which is exclusively sorted in hepatocytes to the apical membrane (Borst and Elferink, 2002). In control

Author Manuscript Author Manuscript Author Manuscript Author Manuscript

polarized hepatocytes, Golgi is localized between the nucleus and BC structures (Figure 1A, C) (Musat et al., 1993). As we have described in the Materials and Methods, VA-13 cells were treated with EtOH during 72 h postplating. At this time, around 79% of cells appears with fragmented Golgi (Petrosyan et al., 2015a, 2016), with around 32 BC detected per 100 cells. Given that at least two cells may form one BC, this corresponds to around 64% of VA-13 cells developing an apical membrane. Importantly, EtOH-induced Golgi fragmentation was equally detected in both polarized and non-polarized VA-13 cells (Figure 1A-D), suggesting that the effect EtOH has on Golgi does not interfere with cells polarization (Figure 1E). Further, Golgi disorganization was also detected in the liver sections from EtOH-fed rats (Figure 1F). Our data fit well with the previous observations indicating that alcohol dramatically alters Golgi architecture (Renau-Piqueras et al., 1985, 1987; Zimmerman, 1999), however earlier observations suggested that chronic EtOH treatment resulted in enlargement of Golgi only (Matsuda et al., 1979). We believe that these divergences mainly depend on the period of exposure and dosage of EtOH administration, as well on the microscopy techniques. In recent years, the novel superresolution microscopy approaches allow to create 3D reconstructed images with a lateral resolution approximately twice that of diffraction-limited instruments. Here, we employed structured illumination superresolution microscopy (SIM), which allows us to achieve two-color 3D imaging at ~110 nm resolution.

EtOH treatment results in ASGP-R devoid of sialylated N-glycans and enriched with high mannose-type N-glycans

The maintenance of compact Golgi morphology requires the giantin in the dimer form. Giantin may facilitate Golgi targeting of some enzymes, but also may be dispensable for trafficking of many others. For example, in advanced prostate cancer cells, failure of giantin monomers to be phosphorylated and dimerized hinders Golgi from forming compact morphology, thereby preventing targeting of core 2 N-acetylglucosaminyltransferase-L/1 (C2GnT-L) to the Golgi. However, Galβ1-3GalNAcαSer/Thr:α2-3sialyltransferase 1 (ST3Gal1), which competes with C2GnT-L for core 1 structure, still can reach the Golgi using the alternative site, which is composed of two *cis*-Golgi proteins, GM130 and GRASP65 (Golgi ReAssembly Stacking Protein 65) (Petrosyan et al., 2014). These observations led us to explore the potential of EtOH-induced Golgi fragmentation to prevent targeting of N-glycosylation enzymes. To identify candidate enzymes, we focused on glycosylation of ASGP-R, because: (a) this protein contains N-glycans which are processed and maturated at the Golgi, where high-mannose types are converted to the complex-type oligosaccharides (Shwartz, 1991); and (b) EtOH treatment results in trapping of ASGP-R in the *cis-medial*-Golgi, thus altering ASGP-R occupancy in the plasma membrane (Petrosyan et al., 2015a).

First, to gain a better understanding of the nature of N-glycosylation that occurs in hepatocytes after EtOH treatment, we performed a mass spectrometric analysis of N-glycans on ASGP-R isolated from control and ethanol-treated VA-13 cells and rat hepatocytes. In control VA-13 cells, $Man_5GlcNAc_2$ and $NeuAc_1Gal_1G1cNAc_1Man_5GlcNAc_2$ constituted 32.4 and 8.8% of total N-glycans, respectively. Other N-glycans were terminated with GlcNAc (40.7%) or NeuAc (18.1%) (Figure 2A) (Shwartz, 1991). In EtOH-treated VA-13

Author Manuscript Author Manuscript Author Manuscript Author Manuscript

cells, high mannose-type N-glycans, including $Man_5GlcNAc_2$ and $Man_8GlcNAc_2$, constituted 58.8 and 11.8% of the N-glycans, respectively and complex-type N-glycans terminated with GlcNAc made up 29.4% of the N-glycans (Figure 2B). The N-glycans on ASGP-R isolated from the hepatocytes of control rats are consisted of high mannose-type $Man_5GlcNAc_2$ (68.1%), and complex-type (31.9%) terminated with GlcNAc, Gal or NeuAc (Figure 2C). Alcohol feeding results in $Man_5GlcNAc_2$ content to 91.1% with the remainder being complex-type N-glycans terminated with GlcNAc (Figure 2D). These results show that EtOH treatment causes a shift of the N-glycans on ASGP-R from mature complex-type forms to immature high-mannose glycans, suggesting an incompletion of the oligosaccharides pathway that normally trims Man_8 structure to produce complex and hybrid-type sugars. We hypothesized that the increase of $Man_5GlcNAc_2$ structure in both VA-13 cells and rat hepatocytes is caused by a dysfunction of MGAT1, the enzyme that add a GlcNAc residue to the terminal Man residue of $Man_5GlcNAc_2$.

To further determine whether alteration of the structure of N-glycans associated with ASGP-R may be ascribed to the downregulation of MGAT1, we employed the *Galanthus novel* lectin (GNL), which is highly specific for the terminal alpha-1,3 mannose (α-1,3 Man). Western blot analysis showed that EtOH treatment increased the amounts of ASGP-R pulled down with GNL from VA-13 cells as well as rat hepatocytes (Figure 3A and B). Given that α2-6NeuAc structure is required for binding of ASPG-R to asialoglycoprotein (Paulson et al., 1977), we also monitored the loss of sialylated N-glycans employing the *Sambucus nigra* agglutinin. However, no ASGP-R was pulled down by SNA in both VA-13 cells and rat hepatocytes after EtOH treatment (Figure 3C and D). These results clearly show that the Golgi of both EtOH-treated VA-13 cells and hepatocytes from EtOH-fed rats are enriched with ASGP-R containing terminal α-1,3 Man, an effect generated by the reduced MGAT1 (Figures 3D).

EtOH-induced Golgi fragmentation is accompanied by mistargeting of MGAT1 and an altered sub-Golgi position for both MGAT1 and Man-II

To elucidate the mechanism of the loss of sialylated N-glycans and increase of high mannose-type N-glycans, we examined the effect of EtOH treatment on sub-Golgi localization and the protein levels of the three enzymes involved in the conversion of high mannose-type N-glycans to complex-type, including Man-I, Man-II, and MGAT1. To obtain the detailed sub-Golgi position of these enzymes, we used SIM microscopy. Not surprisingly, in control VA-13 cells, the *cis*-Golgi localized Man-I (Stanley, 2011) was detected mostly segregated with giantin, which predominantly resides in the *medial*-Golgi (Szul and Sztul, 2011; Petrosyan et al., 2012a) (Figures 4A, Ctrl, and D). In addition, Man-II and MGAT1 were detected in the *medial*-Golgi, as judged by Pearson's coefficient of colocalization with giantin (Slusarewicz et al., 1994; Huang et al., 2015) (Figures 4B, C, Ctrl, and D). As we have shown previously, EtOH treatment induces Golgi disorganization; however, these Golgi fragments are still able to form stacks (Petrosyan et al., 2015a). In spite of the robust impact on Golgi architecture, EtOH treatment has no significant effect on Golgi localization of all three enzymes. It is nevertheless important that, while EtOH treatment did not significantly change the position of Man-I (Figures 4A, EtOH, and D), it dramatically shifted the sub-Golgi localization of Man-II and MGAT1 from the *medial*- to the *cis*-Golgi

Author Manuscript Author Manuscript Author Manuscript Author Manuscript

(Figures 4B, C, EtOH; Supplementary Movie S1). Quantification of Pearson's coefficient indicated that the fractions of Man-II and MGAT1 that appeared colocalized with giantin were significantly reduced in cells treated with EtOH (Figure 4D). Furthermore, we observed that in contrast to Man-I and Man-II, the Golgi-specific immunofluorescence (IF) of MGAT1 was reduced after EtOH treatment and partially detected in the ER, as determined by co-staining with ER marker calreticulin (Fig. S1). Next, using Western blotting, we found that in VA-13 cells, EtOH treatment did not affect the level of Man-I and Man-II, but decreased amount of MGAT1 (Figure 4E). Similar to the results obtained in VA-13 cells, the secretion of MGAT1 was strongly inhibited in hepatocytes isolated from EtOH-fed rats (Figure 4F). Further, we found that after 48 h treatment with EtOH the level of MGAT1 did not undergo significant changes, however the level of its ubiquitination was robustly enhanced (Fig. 4G). Finally, treatment of VA-13 cells with proteasome inhibitor MG-132 (5μM, 18 h) resulted in an increase of level of MGAT1, suggesting that this enzyme is degraded through proteasome-mediated pathway (Fig. 4H).

These results led us to conclude that MGAT1, in contrast to Man-I and Man-II, is giantin-sensitive, and that to be delivered to the Golgi, MGAT1 requires a dimerized giantin structure (Petrosyan et al., 2014). This conclusion was confirmed by analysis of the localizations of these enzymes after treatment of VA-13 cells with *GOLGB1* (giantin) siRNAs. As shown in Figures 5A, B and D, Golgi morphology was affected and the level of MGAT1 was reduced upon silencing giantin; however IF intensity of Man-I and Man-II was identical to control (Figure 5E). At the same time, an MGAT1-specific fluorescence signal was reduced, particularly in Golgi membranes lacking giantin, as visualized by 3D SIM microscopy (Figures 5C and E). The calculated Spearman's rank correlation coefficient between Giantin and MGAT1 IF signal was 0.86, indicating that the level of MGAT1 in the Golgi is positively correlated with the content of giantin (Fig. S2A and B). Therefore, here we observed that giantin is required for the Golgi targeting of MGAT1, the phenomenon we previously reported for core 2 enzymes involved in O-glycosylation (Petrosyan et al., 2012a, 2014). The next question, then, is related to the mechanism that underlies the targeting of Man-I and Man-II. Because several glycosyltransferases need both giantin and the GM130-GRASP65 for Golgi delivery, and both GM130 and GRASP65 seem not to be affected by EtOH treatment (Petrosyan et al., 2012a; Petrosyan et al., 2015a), we anticipated that trafficking of both Man-I and Man-II to the Golgi would be impaired in cells transfected with a mixture of giantin and *GOLGA2* (GM130) siRNAs. Indeed, individual silencing GM130 reduces levels for both GM130 and GRASP65 (Petrosyan et al., 2012a) but had only a marginal effect on intra-Golgi level of both Man-I and Man-II. In addition, fluorescence intensity of Man-I and Man-II in cells lacking GM130 and GRASP65 was comparable to that of control (Fig. S3A-D). However, co-silencing giantin and GM130 completely abolished Golgi targeting for these enzymes (Fig. S3A-E). Thus, knockdown (KD) of giantin induces mislocalization of MGAT1, but not Man-I and Man-II (Figure 5F).

Depletion of MGAT1 is dispensable for trafficking of ASGP-R

Current findings raise the question of whether the phenomenon of EtOH-specific ASGP-R deposition in the Golgi (Petrosyan et al., 2015a) is a consequence of altered Golgi trafficking of MGAT1 or of its downregulation. Therefore, we analyzed in VA-13 cells the plasma

Author Manuscript Author Manuscript Author Manuscript Author Manuscript

membrane content of ASGP-R after siRNAs-specific silencing of MGAT1. We found that, despite *MGAT1* siRNAs treatment, the cells exhibited normal staining patterns for ASGP-R (Fig. S4), and the amount of this protein in the plasma membrane fraction was identical to the cells treated with control siRNAs (Fig. S4). These results demonstrate that an under-glycosylated receptor is still able to reach its final destination and indicate that the function of MGAT1 is dispensable for trafficking of ASGP-R.

EtOH treatment alters intra-Golgi trafficking of COPI vesicles through inhibition of Arf1 activation

As we mentioned in the Introduction, both cisternal maturation and vesicular models seem controversial and do not provide all answers to the current observations (Martinez-Menarguez, 2013). Indeed, the data described above indicate that EtOH treatment arrests Golgi enzymes in the *cis*-Golgi, which cannot be interpreted by either vesicular nor maturation theory. In light of this, we suggested that COPI may also carry Golgi enzymes in the anterograde (from *cis*- to the *medial*-compartments) direction, and that EtOH results in dysfunction of COPI, thus blocking delivery of enzymes to their proper Golgi compartments.

First, at the electron microscopy level, we examined COPI vesiculation by visualization of vesicles budding from the Golgi rims (Rabouille and Klumperman, 2005). In control VA-13 cells (Figure 5G), they were detected on the rims of both *cis-medial*- (inset a) and *trans*-Golgi (inset b). The average number of vesicles varied from three to five per Golgi stack (Figure 5I). In EtOH-treated cells (Figure 5H), the Golgi is predictably fragmented, and the number of COPI-coated vesicles that appeared to emanate from the rims of Golgi cisternae was limited (insert c) or lacking (insert d) (Figure 5H). Overall, the ultrastructural analysis strongly suggests that EtOH interferes with the generation of COPI vesicles, resulting in an abnormally low number of rim-associated, cisternal budding profiles (Figure 5I).

Second, in agreement with the observation that Man-II and MGAT1 have been detected in the COPI vesicles (Gilchrist et al., 2006), we found by high-resolution SIM imaging that both enzymes appeared to partially colocalize in the perinuclear zone with the β-COP, one of the COPI coat subunits (Hsu and Yang, 2009) (Fig. S5A-C; Supplementary Movies S2 and S3), indicating the close association of these enzymes with COPI vesicles. Next, we analyzed whether EtOH treatment abolishes the presence of COPI at the Golgi, using the same antibody to β-COP. In control VA-13 cells, IF staining for β-COP was highly detected at the Golgi, as quantified by Pearson's coefficient of colocalization with giantin (Figures 6A and C, Ctrl). However, as early as after 72 h of exposure to EtOH, the Golgi apparatus manifested significant morphological changes resulting in the dramatic decrease of Golgi-specific β-COP (Figures 6A and C, EtOH). Similarly, in control rat hepatocytes, many β-COP-positive punctae appeared to be at the Golgi area and even more concentrated than that in the VA-13 cells (Figures 6B and C, pair-fed). It was not surprising that in hepatocytes from EtOH-fed rats we observed altered Golgi morphology (Petrosyan et al., 2015a) and β-COP staining predominantly at the cell periphery, but not at the Golgi fragments (Figures 6B and C, EtOH-fed). Next, to validate these results, we measured by Western blot β-COP at the Golgi membranes isolated from these cells. There was a marked decrease of β-COP in

Author Manuscript Author Manuscript Author Manuscript Author Manuscript

the Golgi of both EtOH-treated VA-13 cells and hepatocytes from EtOH-fed rats (Figures 6D and E).

It is known that ADP-ribosylation factor 1 (Arf1) is a key small GTPase that regulates COPI vesicle formation by recruiting coatomer onto Golgi membrane to initiate its coat function (Lee et al., 2005; Hsu and Yang, 2009). Furthermore, *in vitro* analysis suggests that formation of COPI vesicles enriched in Golgi resident proteins is regulated by GTP hydrolysis by Arf1 (Lanoix et al., 2001). Because EtOH treatment induces alteration of COPII vesicles over inactivation of SAR1A (Petrosyan et al., 2015a), we hypothesized that EtOH may also inhibit activation of Arf1. We found that activated Arf1 is reduced after EtOH administration in both VA-13 cells and rat hepatocytes, as determined by Western blot analysis, which showed a decrease of the active GTP-bound form of Arf1 (Figures 6F and G). These results fit well with the observation that coat formation induced by Arf1 and GTP-γS is inhibited in the presence of EtOH (Ktistakis et al., 1996). Thus, we reasoned that the deficiency in β-COP at the Golgi induced by EtOH treatment is triggered by blocking Arf1 activation.

Knockdown of β-COP or overexpression of dominant negative mutant forms of Arf1 mimics the effect of EtOH

To directly address the role of COPI deficiency in regulating the sub-Golgi distribution of early N-glycan biosynthesis enzymes, we analyzed localization of MGAT1 and Man-II in cells lacking β-COP after siRNAs treatment. The first series of experiments was performed using the Zeiss LSM 800 Confocal Laser Microscope with the Airyscan module, which delivers 1.7 times higher resolution and higher sensitivity than conventional confocal microscopes. As shown in Figures 7A and B, in VA-13 cells treated with scrambled siRNAs, the MGAT1 IF signal was widely colocalized with giantin, confirming its *medial*-Golgi position, but mostly segregated from *cis*-Golgi marker, GM130 (Nakamura et al., 1995). However, cells treated with mix of scrambled siRNAs and EtOH exhibited colocalization of MGAT1 and GM130, supporting the idea that MGAT1 dislocates to the *cis*-Golgi in response to Golgi disorganization (Figure 7B, EtOH). Further, as expected, treatment of VA-13 cells with β-COP siRNAs results in anticipated loss of juxtanuclear Golgi complex staining (Petrosyan and Cheng, 2013) (Fig. S6A and B) and the appearance of multiple Golgi fragments which were co-stained with both MGAT1 and GM130 (Figures 7B, *COPB* siRNAs and G). We extended this test by 3D SIM imaging and statistically analyzed the average of distance between identical IF-labeled green and red spots, as described in Materials and Methods. As we have shown previously, the maximal luminal widths of Golgi cisternae determined by electron microscopy are around 120 nm in control, and 275 nm in EtOH-treated VA-13 cells (Petrosyan et al., 2015a), suggesting that IF-stained green and red punctae less than 275 nm apart may be interpreted as a staining within the same Golgi cisterna. In β-COP siRNAs-treated cells, the average distance MGAT1↔giantin was around 795 ± 55 nm (Figures 7C and F; Supplementary Movie S4), while this parameter between MGAT1 and GM130, and MGAT1 and other *cis*-Golgi marker, GRASP65 (Barr et al., 1997), was substantially lower, around 102 ± 48 nm and 85 ± 35 nm, respectively (Figures 7D-F; Supplementary Movies S5 and S6).

Author Manuscript Author Manuscript Author Manuscript Author Manuscript

We then quantitatively analyzed the localization of Man-II before and after β-COP KD. In control cells, 3D SIM imaging reflected the results described in Figure 4B: Man-II is localized in *medial*-Golgi, given that an average of maximal distance Man-II↔giantin did not exceed 125 nm (101 ± 24 nm) (Figures 8A and E), and the gap between Man-II and GRASP65 IF punctae was around 850 ± 19 nm (Figures 8B and E). Similarly to MGAT1, β-COP KD redistributed Man-II to *cis*-compartments, and an average of maximal distance was 730 ± 45 for Man-II↔giantin and 120 ± 30 nm for GRASP65↔Man-II (Figures 8C-E).

We next asked whether overexpression of the inactive GDP-bound, dominant-negative mutant of Arf1, Arf1(T31N) (Moorhead et al., 2010), would affect the sub-Golgi position for both Man-II and MGAT1. Consistent with the observation of others (Ward et al., 2001), we found that in VA-13 cells transfected with Arf1(T31N) plasmid, Golgi undergoes morphological transformation identical to the one we observed after β-COP KD (Figures 8F-I). Whereas in control cells (transfected with empty pcDNA3.1 vector) the average IF distance was around 965 ± 20 nm for GRASP65↔Man-II and 972 ± 18 nm for GRASP65↔MGAT1, in cells that overexpressed Arf1(T31N), this parameter was robustly reduced to 82 ± 24 nm for GRASP65↔Man-II and 93 ± 20 nm for GRASP65↔MGAT1 (Figures 8F-J; Supplementary Movie S7). Thus, we reasoned that impairment of COPI vesicle formation (either after β-COP KD or overexpression of Arf1(T31N) results in *medial*-to-*cis* relocation of two N-glycosylation enzymes, Man-II and MGAT1, the same phenomenon we observed after EtOH treatment.

DISCUSSION

The close relationship between Golgi matrix and non-matrix proteins is the key determinant for Golgi integrity. Whereas the function of matrix proteins, including golgins (GM130, giantin etc.) and GRASPs is increasingly being viewed as essential for proper glycosylation (Puthenveedu et al., 2006; Petrosyan et al., 2012a; Xiang et al., 2013), little is known about the role of these proteins in EtOH-related aberrant glycosylation. In this report, we have shown that EtOH-induced Golgi fragmentation in hepatocytes results in alteration of Golgi trafficking of the key N-glycosylation enzyme MGAT1, which leads to its degradation and the subsequent abnormal N-glycosylation.

It has been proposed that COPI vesicles may carry both resident Golgi proteins and secretory cargos in ER-to-Golgi direction (Pelham and Rothman, 2000). However, we and others have found that glycosyltransferases are transported as a part of vesicular or tubular complexes, which sizes were much more than that of reported COPI vesicles (20-60 nm) (Martinez-Alonso et al., 2005; Petrosyan et al., 2012a). Notably, depletion of β-COP did not abolish the transportation of these complexes to the Golgi. Thus, the open questions are what the nature of these structures, and how they are transported to the Golgi. Also, it is important to note that we previously found that glycosyltransferases employ heterogeneous Golgi targeting mechanisms, using either giantin or GM130-GRASP65 as the primary docking sites (Petrosyan et al., 2012a). We also showed that the giantin-dependent mechanism is lacking in advanced prostate cancer, and this trait cardinally modifies O-glycan elongation by virtue of the domination of pathways mediated by giantin-independent glycosyltransferases (Petrosyan et al., 2014). Here, we show that administration of EtOH

Author Manuscript Author Manuscript Author Manuscript Author Manuscript

and the subsequent impaired dimerization of giantin (Petrosyan et al., 2015a) affect the level of MGAT1 in the Golgi. Further, in cells lacking giantin after siRNAs treatment, this enzyme was depleted from Golgi, indicating that presence of giantin is prerequisite for successful Golgi targeting of MGAT1. Also, it is interesting to note that EtOH has no effect on the level or Golgi localization of two glycosidases, Man-I and Man-II, despite Golgi disorganization. This singularity implies that these two N-glycan processing enzymes may employ alternative Golgi targeting mechanisms. Indeed, we revealed that the presence of Man-I and Man-II in the Golgi requires either giantin or the GM130-GRASP65 complex. In addition, our data suggest that the level of Golgi resident proteins may be impaired by two sequential mechanisms: (a) the blocking of their Golgi targeting (Figure 9); and (b) the increase of their Golgi-to-cytoplasm transportation, followed by proteasomal degradation (Petrosyan et al., 2012b). The latter coincides with Golgi fragmentation, which is provided by Rab6a-mediated cooperation of non-muscle Myosin IIA with the cytoplasmic tail of other Golgi enzymes (Petrosyan et al., 2012b; Petrosyan and Cheng, 2013, 2014; Petrosyan et al., 2016), of which Golgi localization is not affected by EtOH. While we and others have shown the role of the cytoplasmic tail for Golgi retention of glycosyltransferases (Banfield et al., 2011; Ali et al., 2012; Petrosyan et al., 2015b), it is still unclear whether during Golgi targeting the cytoplasmic tail interacts directly with Golgi matrix proteins and whether such a link is sequence-dependent. Also, we do not rule out that in addition to suggested pathways, EtOH treatment may also affect function of Golgi enzymes through alteration of their Golgi retention mechanism or activation of proteins which potentially may inhibit their function in the Golgi (Huang et al., 2015). These possibilities need further rigorous studies.

EtOH appears to specifically alter N-glycan modification on ASGP-R; however, abnormal glycosylation cannot be considered as the cause of its impaired transportation, because depletion of MGAT1 in hepatocytes has no effect on the presence of ASGP-R in the plasma membrane. In the meantime, we wish to highlight that the minimal fraction of ASGP-R, which could be detected in the plasma membrane after EtOH administration, has reduced binding capacity (Casey et al., 1987). This phenomenon can be explained by the loss of sialylated N-glycans on ASGP-R, because the presence of α2,6NeuAc is stringent requirement for endocytosis of asialoglycoproteins (Paulson et al., 1977). Thus, the answer to the question of how EtOH-induced Golgi fragmentation results in accumulation of ASGP-R in the *cis-medial*-Golgi (Petrosyan et al., 2015a) may reside in the altered intra-Golgi transportation of ASGP-R rather than in the defects of its glycosylation. Also, the seemingly remote possibility that COPI may carry ASGP-R during transiting through Golgi, because in our study, in both VA-13 cells and rat hepatocytes, despite COPI deficiency, ASGP-R is still able to reach the *medial*-Golgi.

Given that MGAT1 has an essential role in N-glycosylation, it is reasonable to anticipate that ASGP-R is not the only glycoprotein bearing high-mannose-type sugars that is affected by EtOH. Indeed, recent analysis of N-glycans in liver-secreted protein fractions from cirrhosis patients, including alcoholic, revealed an increase in high-mannose structures (Bekesova et al., 2012). However, ASGP-R is a transmembrane protein, and the phenomenon of its deposition in the *cis-medial*-Golgi cannot necessarily be applied to the wide range of secreted glycoproteins. These proteins may employ distinct machinery to target the plasma membrane, and under-glycosylation may or may not be accompanied by impairment in

Author Manuscript Author Manuscript Author Manuscript Author Manuscript

secretion. A good example is the carbohydrate-deficient form of transferrin, which is still partially secreted into the blood and serves as an excellent test for monitoring compliance of alcohol consumption (Bell et al., 1993). Thus, the fragments of Golgi stacks are still potentially capable of transporting proteins, and the fundamental question that arises is why EtOH-induced Golgi partitioning is dispensable for trafficking of certain proteins, but is critical for others.

We observed that EtOH treatment impairs formation of COPI vesicles, and KD of β-COP or transfection of cells with Arf1(T31N) cDNA reproduce the effect of EtOH, as evident in the translocation of MGAT1 and Man-II to the *cis*-Golgi. Thus, we would like to underscore the existence of two synchronous EtOH-induced alterations of vesicular trafficking: (a) the reduced targeting of MGAT1 to the fragmented Golgi, which is initiated by COPII impairment followed by deficiency in giantin; and (b) abnormal sub-Golgi location of MGAT1 and Man-II caused by lack of COPI (Figure 9). The important question, then, is whether such a translocation of Golgi enzymes may have an effect on N-glycosylation. The evidences that β-COP depletion arrests not only anterograde trafficking of selected glycoproteins but also their glycosylation (Styers et al., 2008) suggest that this would be the case.

Another important conclusion is a comparison of EtOH-induced Golgi fragmentation with Golgi scattering induced by the microtubule depolymerization agent Nocodazole. Recent quantitative analysis by imaging centers of mass indicate that multiple Nocodazole-induced Golgi fragments still preserve stacking; however, contrary to EtOH treatment, they maintain differential (from *cis*-to-*trans*-Golgi) distribution of enzymes (Tie et al., 2016). Most importantly, Nocodazole does not alter either intra-Golgi localization of COPI nor glycosylation of glycoproteins (Beske et al., 2007; Xiang et al., 2013). Thus, it is attractive to speculate that EtOH-induced abnormal glycosylation and COPI/COPII dysfunction are two sides of the same coin. On the face of it, one might conclude from this that the effect EtOH has on intracellular trafficking is multitarget. However, we should admit that alcohol treatment still remains one of the most “physiological” models to study intracellular alterations. Luckily, we are entering a new era of superresolution imaging, and new unprecedented possibilities may open many doors for uncovering the mysteries of intracellular trafficking.

Supplementary Material

Refer to Web version on PubMed Central for supplementary material.

ACKNOWLEDGMENTS

We acknowledge Dr. Adrian E. Koesters for critical review of the manuscript. Support for the UNMC Advanced Microscopy Core Facility was provided by the Nebraska Research Initiative, the Fred and Pamela Buffett Cancer Center Support Grant (P30CA036727), and an Institutional Development Award (IDeA) from the NIGMS of the NIH (P30GM106397). This research was supported by the K01AA022979-01 award from the National Institute on Alcohol and Alcohol Abuse (to A.P.).

Author Manuscript Author Manuscript Author Manuscript Author Manuscript

REFERENCES

Ali MF, Chachadi VB, Petrosyan A, Cheng PW. Golgi phosphoprotein 3 determines cell binding properties under dynamic flow by controlling Golgi localization of core 2 N-acetylglucosaminyltransferase 1. J Biol Chem. 2012; 287:39564–39577. [PubMed: 23027862]

Asante D, Maccarthy-Morrogh L, Townley AK, Weiss MA, Katayama K, Palmer KJ, Suzuki H, Westlake CJ, Stephens DJ. A role for the Golgi matrix protein giantin in ciliogenesis through control of the localization of dynein-2. J Cell Sci. 2013; 126:5189–5197. [PubMed: 24046448]

Bacallao R, Antony C, Dotti C, Karsenti E, Stelzer EH, Simons K. The subcellular organization of Madin-Darby canine kidney cells during the formation of a polarized epithelium. J Cell Biol. 1989; 109:2817–2832. [PubMed: 2592406]

Banfield DK. Mechanisms of protein retention in the Golgi. Cold Spring Harb Perspect Biol. 2011; 3(8):a005264. doi: 10.1101/cshperspect.a005264. [PubMed: 21525512]

Barr FA, Puype M, Vandekerckhove J, Warren G. GRASP65, a protein involved in the stacking of Golgi cisternae. Cell. 1997; 91:253–262. [PubMed: 9346242]

Bekesova S, Kosti O, Chandler KB, Wu J, Madej HL, Brown KC, Simonyan V, Goldman R. N-glycans in liver-secreted and immunoglogulin-derived protein fractions. J Proteomics. 2012; 75:2216–2224. [PubMed: 22326963]

Bell H, Tallaksen C, Sjaheim T, Weberg R, Raknerud N, Orjasaeter H, Try K, Haug E. Serum carbohydrate-deficient transferrin as a marker of alcohol consumption in patients with chronic liver diseases. Alcohol Clin Exp Res. 1993; 17:246–252. [PubMed: 8488962]

Beske O, Reichelt M, Taylor MP, Kirkegaard K, Andino R. Poliovirus infection blocks ERGIC-to-Golgi trafficking and induces microtubule-dependent disruption of the Golgi complex. J Cell Sci. 2007; 120:3207–3218. [PubMed: 17711878]

Borst P, Elferink RO. Mammalian ABC transporters in health and disease. Annu Rev Biochem. 2002; 71:537–592. [PubMed: 12045106]

Bouma ME, Rogier E, Verthier N, Labarre C, Feldmann G. Further cellular investigation of the human hepatoblastoma-derived cell line HepG2: morphology and immunocytochemical studies of hepatic-secreted proteins. In Vitro Cell Dev Biol. 1989; 25:267–275. [PubMed: 2466823]

Braza-Boils A, Tomas M, Marin MP, Megias L, Sancho-Tello M, Fornas E, Renau-Piqueras J. Glycosylation is altered by ethanol in rat hippocampal cultured neurons. Alcohol Alcohol. 2006; 41:494–504. [PubMed: 16751217]

Casey CA, Kragskow SL, Sorrell MF, Tuma DJ. Chronic ethanol administration impairs the binding and endocytosis of asialo-orosomucoid in isolated hepatocytes. J Biol Chem. 1987; 262:2704–2710. [PubMed: 3818618]

Chiu JH, Hu CP, Lui WY, Lo SC, Chang CM. The formation of bile canaliculi in human hepatoma cell lines. Hepatology. 1990; 11:834–842. [PubMed: 2161394]

Clemens DL, Forman A, Jerrells TR, Sorrell MF, Tuma DJ. Relationship between acetaldehyde levels and cell survival in ethanolmetabolizing hepatoma cells. Hepatology. 2002; 35:1196–1204. [PubMed: 11981770]

Costes SV, Daelemans D, Cho EH, Dobbin Z, Pavlakis G, Lockett S. Automatic and quantitative measurement of protein-protein colocalization in live cells. Biophys J. 2004; 86:3993–4003. [PubMed: 15189895]

Cottalasso D, Gazzo P, Dapino D, Domenicotti C, Pronzato MA, Traverso N, Bellocchio A, Nanni G, Marinari UM. Effect of chronic ethanol consumption on glycosylation processes in rat liver microsomes and Golgi apparatus. Alcohol Alcohol. 1996; 31:51–59. [PubMed: 8672174]

Gilchrist A, Au CE, Hiding J, Bell AW, Fernandez-Rodriguez J, Lesimple S, Nagaya H, Roy L, Gosline SJ, Hallett M, Paiement J, Kearney RE, Nilsson T, Bergeron JJ. Quantitative proteomics analysis of the secretory pathway. Cell. 2006; 127:1265–1281. [PubMed: 17174899]

Gravel P, Walzer C, Aubry C, Balant LP, Yersin B, Hochstrasser DF, Guimon J. New alterations of serum glycoproteins in alcoholic and cirrhotic patients revealed by high resolution two-dimensional gel electrophoresis. Biochem Biophys Res Commun. 1996; 220:78–85. [PubMed: 8602862]

Author Manuscript Author Manuscript Author Manuscript Author Manuscript

Guasch R, Renau-Piqueras J, Guerri C. Chronic ethanol consumption induces accumulation of proteins in the liver Golgi apparatus and decreases galactosyltransferase activity. Alcohol Clin Exp Res. 1992; 16:942–948. [PubMed: 1443433]

Hsu VW, Yang JS. Mechanisms of COPI vesicle formation. FEBS Lett. 2009; 583:3758–3763. [PubMed: 19854177]

Huang HH, Hassinen A, Sundaram S, Spiess AN, Kellokumpu S, Stanley P. GnT1IP-L specifically inhibits MGAT1 in the Golgi via its luminal domain. Elife. 2015 doi: 10.7554/eLife.08916.

Kellokumpu S, Sormunen R, Kellokumpu I. Abnormal glycosylation and altered Golgi structure in colorectal cancer: dependence on intra-Golgi pH. FEBS Lett. 2002; 516:217–224. [PubMed: 11959136]

Koreishi M, Gniadek TJ, Yu S, Masuda J, Honjo Y, Satoh A. The golgin tether giantin regulates the secretory pathway by controlling stack organization within Golgi apparatus. PLoS One. 2013; 8:3. doi: 10.1371/journal.pone.0059821.

Ktistakis NT, Brown HA, Waters MG, Sternweis PC, Roth MG. Evidence that phospholipase D mediates ADP ribosylation factor-dependent formation of Golgi coated vesicles. J Cell Biol. 1996; 134:295–306. [PubMed: 8707816]

Lanoix J, Ouwendijk J, Stark A, Szafer E, Cassel D, Dejgaard K, Weiss M, Nilsson T. Sorting of Golgi resident proteins into different subpopulations of COPI vesicles: a role for ArfGAP1. J Cell Biol. 2001; 155:1199–1212. [PubMed: 11748249]

Lee SY, Yang JS, Hong W, Premont RT, Hsu VW. ARFGAP1 plays a central role in coupling COPI cargo sorting with vesicle formation. J Cell Biol. 2005; 168:281–290. [PubMed: 15657398]

Lieber CS, DeCarli LM. The feeding of alcohol in liquid diets: two decades of applications and 1982 update. Alcohol Clin Exp Res. 1982; 6:523–531. [PubMed: 6758624]

Marinari UM, Pronzato MA, Pizzorno R, Cottalasso D, Maloberti G, Domenicotti C, Gazzo P, Nanni G. Acetaldehyde-induced impairment of protein glycosylation in liver Golgi apparatus. Biochem Mol Biol Int. 1993; 29:1131–1138. [PubMed: 8330019]

Martinez-Alonso E, Egea G, Ballesta J, Martinez-Menarguez JA. Structure and dynamics of the Golgi complex at 15 degrees C: low temperature induces the formation of Golgi-derived tubules. Traffic. 2005; 6:32–44. [PubMed: 15569243]

Martinez-Menarguez J, Prekeris R, Oorschot VM, Scheller R, Slot JW, Geuze HJ, Klumperman J. Peri-Golgi vesicles contain retrograde but not anterograde proteins consistent with the cisternal progression model of intra-Golgi transport. J Cell Biol. 2001; 155:1213–1224. [PubMed: 11748250]

Martinez-Menarguez J. Intra-golgi transport: roles for vesicles, tubules, and cisternae. ISRN Cell Biol. 2013 doi: 10.1155/2013/126731.

Matsuda Y, Baraona E, Salaspuro M, Lieber CS. Effects of ethanol on liver microtubules and Golgi apparatus. Possible role in altered hepatic secretion of plasma proteins. Lab Invest. 1979; 41:455–463. [PubMed: 502475]

Mee CJ, Harris HJ, Farquhar MJ, Wilson G, Reynolds G, Davis C, van IJzendoorn SC, Balfe P, McKeating JA. Polarization restricts hepatitis C virus entry into HepG2 hepatoma cells. J Virol. 2009; 83:6211–6221. [PubMed: 19357163]

Mironov AA, Weidman P, Luini A. Variations on the intracellular transport theme: maturing cisternae and trafficking tubules. J Cell Biol. 1997; 138:481–484. [PubMed: 9245779]

Moorhead AM, Jung JY, Smirnov A, Kaufer S, Scidmore MA. Multiple host proteins that function in phosphatidylinositol-4-phosphate metabolism are recruited to the chlamydial inclusion. Infect Immun. 2010; 78:1990–2007. [PubMed: 20231409]

Morelle W, Michalski JC. Analysis of protein glycosylation by mass spectrometry. Nat Protoc. 2007; 2:1585–1602. [PubMed: 17585300]

Musat AI, Sattler CA, Sattler GL, Pitot HC. Reestablishment of cell polarity of rat hepatocytes in primary culture. Hepatology. 1993; 18:198–205. [PubMed: 8325611]

Nakamura N, Rabouille C, Watson R, Nilsson T, Hui N, Slusarewicz P, Kreis TE, Warren G. Characterization of a cis-Golgi matrix protein, GM130. J Cell Biol. 1995; 131:1715–1726. [PubMed: 8557739]

Author Manuscript Author Manuscript Author Manuscript Author Manuscript

NIAAA. National Institute on Alcohol Abuse and Alcoholism. Liver cirrhosis mortality in the United States: national, state, and regional trends, 2000-2011. 2014.

Orci L, Stamnes M, Ravazzola M, Amherdt M, Perrelet A, Söllner TH, Rothman JE. Bidirectional transport by distinct populations of COPI-coated vesicles. Cell. 1997; 90:335–349. [PubMed: 9244307]

Orci L, Ravazzola M, Volchuk A, Engel T, Gmachl M, Amherdt M, Perrelet A, Sollner TH, Rothman JE. Anterograde flow of cargo across the golgi stack potentially mediated via bidirectional "percolating" COPI vesicles. Proc Natl Acad Sci U S A. 2000; 97:10400–10405. [PubMed: 10962035]

Paulson JC, Hill RL, Tanabe T, Ashwell G. Reactivation of asialo-rabbit liver binding protein by resialylation with beta-D-galactoside alpha2 leads to 6 sialyltransferase. J Biol Chem. 1977; 10:8624–8628.

Pelham HR, Rothman JE. The debate about transport in the Golgi--two sides of the same coin? Cell. 2000; 102:713–719. [PubMed: 11030615]

Petrosyan A, Ali MF, Cheng PW. Glycosyltransferase-specific Golgi-targeting mechanisms. J Biol Chem. 2012; 287:37621–37627. [PubMed: 22988244]

Petrosyan A, Ali MF, Verma SK, Cheng H, Cheng PW. Non-muscle myosin IIA transports a Golgi glycosyltransferase to the endoplasmic reticulum by binding to its cytoplasmic tail. Int J Biochem Cell Biol. 2012; 44:1153–1165. [PubMed: 22525330]

Petrosyan A, Cheng PW. A non-enzymatic function of Golgi glycosyltransferases: mediation of Golgi fragmentation by interaction with non-muscle myosin IIA. Glycobiology. 2013; 23:690–708. [PubMed: 23396488]

Petrosyan A, Holzapfel MS, Muirhead DE, Cheng PW. Restoration of compact Golgi morphology in advanced prostate cancer enhances susceptibility to galectin-1-induced apoptosis by modifying mucin O-glycan synthesis. Mol Cancer Res. 2014; 12:1704–1716. [PubMed: 25086069]

Petrosyan A, Cheng PW. Golgi fragmentation induced by heat shock or inhibition of heat shock proteins is mediated by non-muscle myosin IIA via its interaction with glycosyltransferases. Cell Stress Chaperones. 2014; 19:241–254. [PubMed: 23990450]

Petrosyan A, Cheng PW, Clemens DL, Casey CA. Downregulation of the small GTPase SAR1A: a key event underlying alcohol-induced Golgi fragmentation in hepatocytes. Sci Rep. 2015; 5:17127. doi: 10.1038/srep17127. [PubMed: 26607390]

Petrosyan A, Ali MF, Cheng PW. Keratin 1 plays a critical role in Golgi localization of Core 2 N-acetylglucosaminyltransferase M via interaction with its cytoplasmic tail. J Biol Chem. 2015; 290:6256–6269. [PubMed: 25605727]

Petrosyan A. Onco-Golgi: Is Fragmentation a Gate to Cancer Progression? Biochem Mol Biol J. 2015; 1:1–6.

Petrosyan A, Casey CA, Cheng PW. The role of Rab6a and phosphorylation of non-muscle myosin IIA tailpiece in alcohol-induced Golgi disorganization. Sci Rep. 2016; 18:6–31962. doi: 10.1038/srep31962.

Pokrovskaya ID, Willett R, Smith RD, Morelle W, Kudlyk T, Lupashin VV. Conserved oligomeric Golgi complex specifically regulates the maintenance of Golgi glycosylation machinery. Glycobiology. 2011; 21:1554–1569. [PubMed: 21421995]

Puthenveedu MA, Bachert C, Puri S, Lanni F, Linstedt AD. GM130 and GRASP65-dependent lateral cisternal fusion allows uniform Golgi-enzyme distribution. Nat Cell Biol. 2006; 8:238–248. [PubMed: 16489344]

Rabouille C, Klumperman J. Opinion: The maturing role of COPI vesicles in intra-Golgi transport. Nat Rev Mol Cell Biol. 2005; 6:812–817. [PubMed: 16167055]

Renau-Piqueras J, Gomez-Perretta C, Guerri C, Sanchis R. Qualitative and quantitative ultrastructural alterations in hepatocytes of rats prenatally exposed to ethanol with special reference to mitochondria, golgi apparatus and peroxisomes. Virchows Arch A Pathol Anat Histopathol. 1985; 405:237–251. [PubMed: 3918388]

Renau-Piqueras J, Miragall F, Guerri C, Baguena-Cervellera R. Prenatal exposure to alcohol alters the Golgi apparatus of newborn rat hepatocytes: a cytochemical study. J Histochem Cytochem. 1987; 35:221–228. [PubMed: 3025292]

Author Manuscript Author Manuscript Author Manuscript Author Manuscript

Sagi D, Kienz P, Denecke J, Marquardt T, Peter-Katalinic J. Glycoproteomics of N-glycosylation by in-gel deglycosylation and matrix-assisted laser desorption/ionisation-time of flight mass spectrometry mapping: application to congenital disorders of glycosylation. Proteomics. 2005; 5:2689–2701. [PubMed: 15912511]

Schaffert CS, Sorrell MF, Tuma DJ. Expression and cytoskeletal association of integrin subunits is selectively increased in rat perivenous hepatocytes after chronic ethanol administration. Alcohol Clin Exp Res. 2001; 25:1749–1757. [PubMed: 11781508]

Shevchenko A, Tomas H, Havlis J, Olsen JV, Mann M. In-gel digestion for mass spectrometric characterization of proteins and proteomes. Nat Protoc. 2006; 1:2856–2860. [PubMed: 17406544]

Shwartz, A. Trafficking of asialoglycoproteins and the asialoglycoprotein receptor. In: Wu, GY.; Wu, CY., editors. Liver Diseases: Targeted Diagnosis and Therapy Using Specific Receptors and Ligands. Marcel Dekker; New York: 1991. p. 3-41.Ch. 1

Slusarewicz P, Nilsson T, Hui N, Watson R, Warren G. Isolation of a matrix that binds medial Golgi enzymes. J Cell Biol. 1994; 124:405–413. [PubMed: 8106542]

Sormunen R, Eskelinen S, Lehto VP. Bile canaliculus formation in cultured HEPG2 cells. Lab Invest. 1993; 68:652–662. [PubMed: 8390592]

Stanley P. Golgi glycosylation. Cold Spring Harb Perspect Biol. 2011; 3:a005199. doi: 10.1101/cshperspect.a005199. [PubMed: 21441588]

Styers ML, O'Connor AK, Grabski R, Cormet-Boyaka E, Sztul E. Depletion of beta-COP reveals a role for COP-I in compartmentalization of secretory compartments and in biosynthetic transport of caveolin-1. Am J Physiol Cell Physiol. 2008; 294:C1485–1498. [PubMed: 18385291]

Szul T, Sztul E. COPII and COPI traffic at the ER-Golgi interface. Physiology. 2011; 26:348–364. [PubMed: 22013193]

Theard D, Steiner M, Kalicharan D, Hoekstra D, van Ijzendoorn SC. Cell polarity development and protein trafficking in hepatocytes lacking E-cadherin/beta-catenin-based adherens junctions. Mol Biol Cell. 2007; 18:2313–2321. [PubMed: 17429067]

Tie HC, Mahajan D, Chen B, Cheng L, VanDongen AM, Lu L. A novel imaging method for quantitative Golgi localization reveals differential intra-Golgi trafficking of secretory cargoes. Mol Biol Cell. 2016; 27:848–861. [PubMed: 26764092]

Tworek BL, Tuma DJ, Casey CA. Decreased binding of asialoglycoproteins to hepatocytes from ethanol-fed rats. Consequence of both impaired synthesis and inactivation of the asialoglycoprotein receptor. J Biol Chem. 1996; 271:2531–2538. [PubMed: 8576217]

Van IJzendoorn SC, Zegers MM, Kok JW, Hoekstra D. Segregation of glucosylceramide and sphingomyelin occurs in the apical to basolateral transcytotic route in HepG2 cells. J Cell Biol. 1997; 137:347–357. [PubMed: 9128247]

Van IJzendoorn SC, Van Der Wouden JM, Liebisch G, Schmitz G, Hoekstra D. Polarized membrane traffic and cell polarity development is dependent on dihydroceramide synthase-regulated sphinganine turnover. Mol Biol Cell. 2004; 2004; 15(9):4115–4124. [PubMed: 15229289]

Ward TH, Polishchuk RS, Caplan S, Hirschberg K, Lippincott-Schwartz J. Maintenance of Golgi structure and function depends on the integrity of ER export. J Cell Biol. 2001; 155:557–570. [PubMed: 11706049]

Waszkiewicz N, Szajda SD, Zalewska A, Szulc A, Kępka A, Minarowska A, Wojewódzka-Żelezniakowicz M, Konarzewska B, Chojnowska S, Ladny JR, Zwierz K. Alcohol abuse and glycoconjugate metabolism. Folia Histochem Cytobiol. 2012; 50:1–11. [PubMed: 22532130]

Xiang Y, Zhang X, Nix DB, Katoh T, Aoki K, Tiemeyer M, Wang Y. Regulation of protein glycosylation and sorting by the Golgi matrix proteins GRASP55/65. Nat Commun. 2013; 4:1659. doi: 10.1038/ncomms2669. [PubMed: 23552074]

Zaal KJ, Kok JW, Sormunen R, Eskelinen S, Hoekstra D. Intracellular sites involved in the biogenesis of bile canaliculi in hepatic cells. Eur J Cell Biol. 1994; 63:10–19. [PubMed: 8005096]

Zegers MM, Hoekstra D. Sphingolipid transport to the apical plasma membrane domain in human hepatoma cells is controlled by PKC and PKA activity: a correlation with cell polarity in HepG2 cells. J Cell Biol. 1997; 138:307–321. [PubMed: 9230073]

Author Manuscript Author Manuscript Author Manuscript Author Manuscript

Zegers MM, Zaal KJ, van IJzendoorn SC, Klappe K, Hoekstra D. Actin filaments and microtubules are involved in different membrane traffic pathways that transport sphingolipids to the apical surface of polarized HepG2 cells. Mol Biol Cell. 1998; 9:1939–1949. [PubMed: 9658181]

Zimmerman, HJ. Hepatotoxic effects of ethanol. In: Zimmerman, HJ., editor. Hepatotoxicity: The Adverse Effects of Drugs and Other Chemicals on the Liver. 2nd ed.. Lippincott Williams & Wilkins; Philadelphia: 1999. p. 147-177.

Author Manuscript Author Manuscript Author Manuscript Author Manuscript

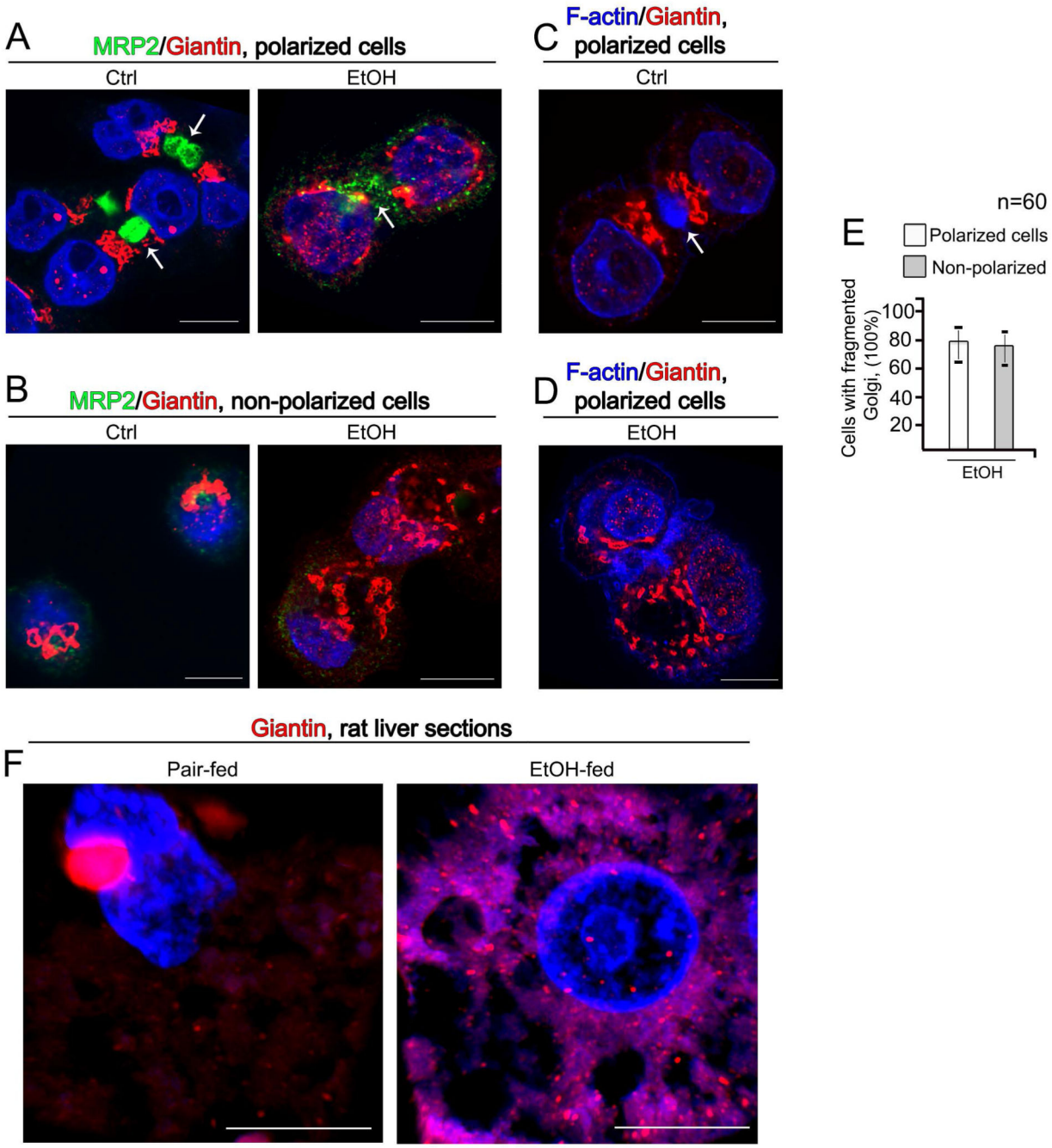

Figure 1.

(A, B) Immunostaining of MRP2 (green) and giantin (red) in polarized (A) and non-polarized (B) VA-13 cells before and after treatment with 35 mM EtOH for 72 h. Nuclei were counterstained with DAPI (blue). (C, D) F-actin staining (blue) and immunostaining of giantin (red) in polarized VA-13 cells before (C) and after treatment with 35 mM EtOH for 72 h (D). BC are indicated by white arrow. All confocal images were acquired with the same imaging parameters; bars, 10 μm. (E) Quantification of cells with fragmented Golgi in EtOH-treated VA-13 polarized vs. non-polarized cells. Results are expressed as a mean ±

SD; n = 60 cells from two independent experiments. (F) Representative cells from liver sections of pair-fed or EtOH-fed rats. Sections were stained with giantin (red), and nuclei were counterstained with DAPI (blue); bars 5 μm. 3D reconstruction of images were obtained using SM 800 Confocal Laser Microscope with the Airyscan module.

Author Manuscript Author Manuscript Author Manuscript Author Manuscript

Author Manuscript
Author Manuscript
Author Manuscript
Author Manuscript

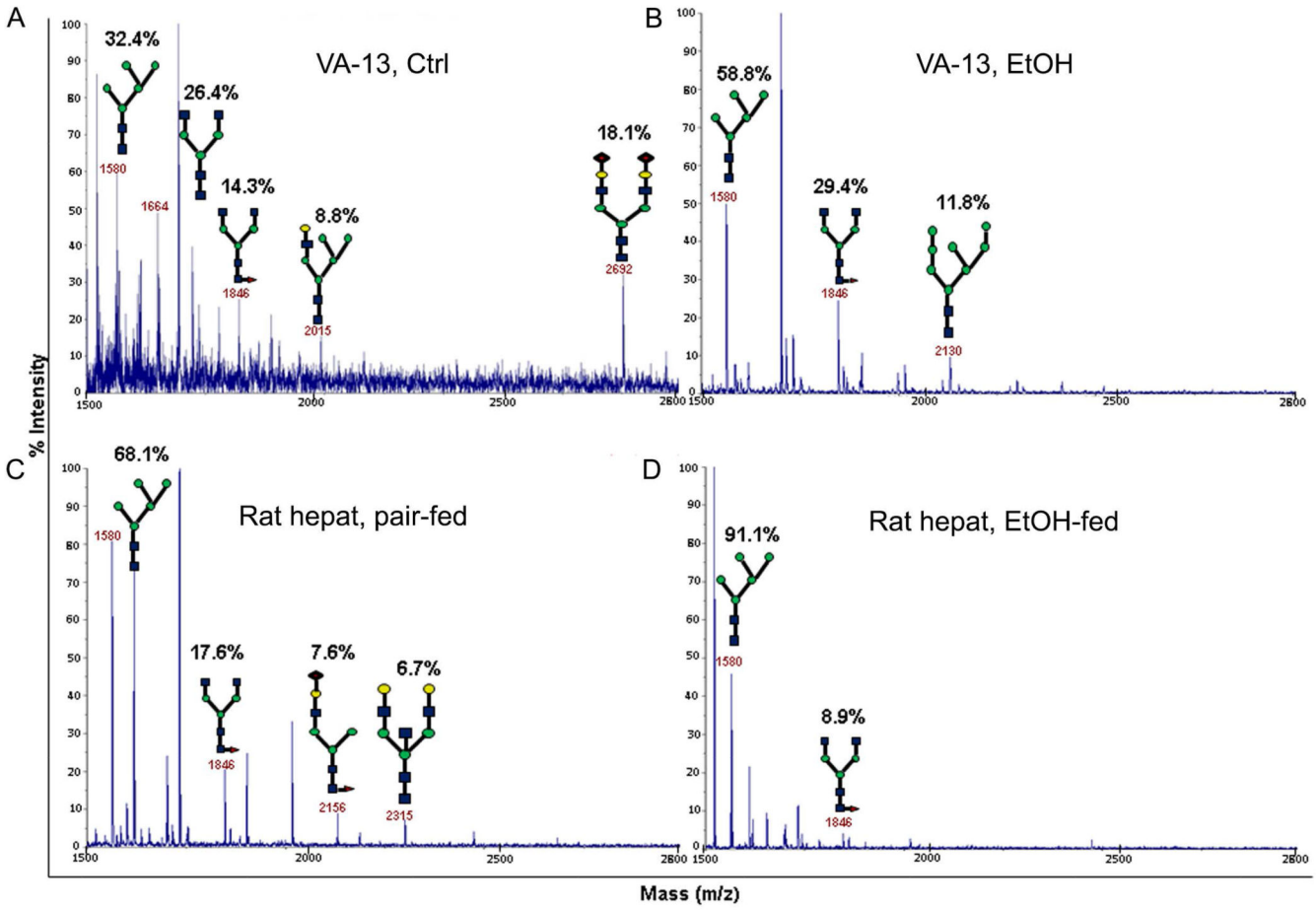

Figure 2.

MALDI-TOF analysis of N-glycans on ASGP-R isolated from control (A) and EtOH-treated VA-13 cells (B), pair-fed rat hepatocytes (C) and hepatocytes from EtOH-fed rats (D). The structural assignments were made based on the MALDI mass and MS-MS experiments. Each N-glycan is expressed as % of total N-glycans within each sample. Symbols: Gal, yellow circles; Man, green circles; GlcNAc, blue squares; Fuc, orange triangles; Sia, red diamonds.

Author Manuscript Author Manuscript Author Manuscript Author Manuscript

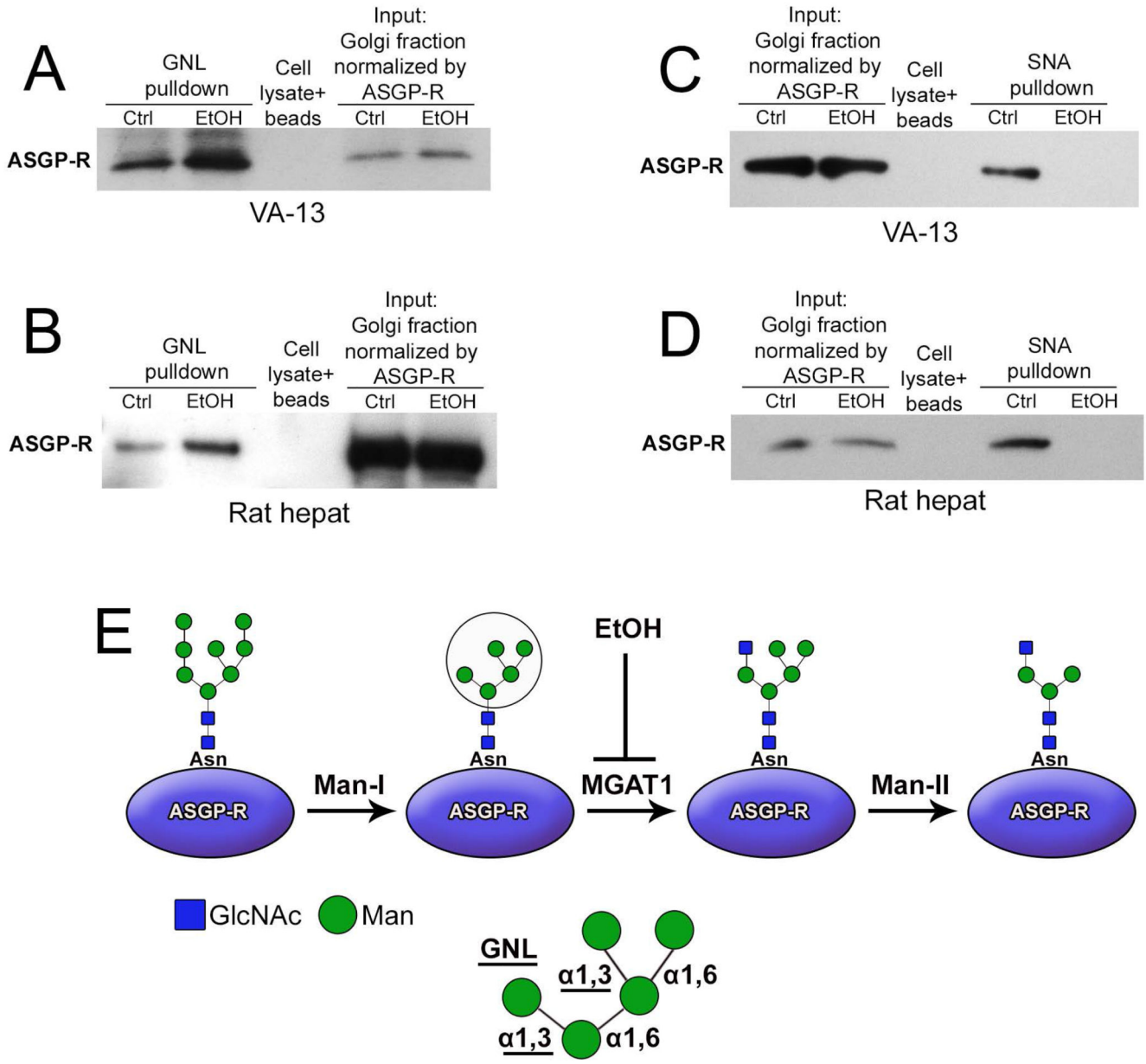

Figure 3.

Altered glycosylation of ASGP-R in cells treated with EtOH. (A, B) ASGP-R western blot of GNL pulldown from 20 μg Golgi fraction of VA-13 cells shown in panel A. ASGP-R western blot of GNL pulldown from 35 μg Golgi fraction of rat hepatocytes shown in panel B. (C, D) ASGP-R western blot of the SNA lectin pulldown from 20 μg Golgi fraction of VA-13 cells shown in panel C. ASGP-R western blot of the SNA pulldown from 35 μg Golgi fraction of rat hepatocytes shown in panel D. Golgi fraction was incubated with biotinylated GNL (A and B) or SNA lectin (C and D), followed by pull-down with streptavidin magnet beads. The beads exposed to lysate served only as a control. The results shown are representative of three independent experiments. (E) Schema of ASGP-R-specific N-linked high-mannose oligosaccharides pathway. The $(Man)_5(GlcNAc)_2$ structure occurs after

Author Manuscript Author Manuscript Author Manuscript Author Manuscript

trimming by Mannosidase I (α-1,2 specific), then MGAT1 adds a N-acetylglucosamine residue to the terminal Man residue followed by the action of Mannosidase II (α-1,3/6 specific) to remove two Man residues. Further processing (not shown) results in the continued synthesis of complex type oligosaccharides. EtOH administration presumably leads to down-regulation of MGAT1 and formation of ASGP-R-associated N-glycans terminated with α-1,3 Man detected with GNL (in circle, and highlighted below).

Author Manuscript Author Manuscript Author Manuscript Author Manuscript

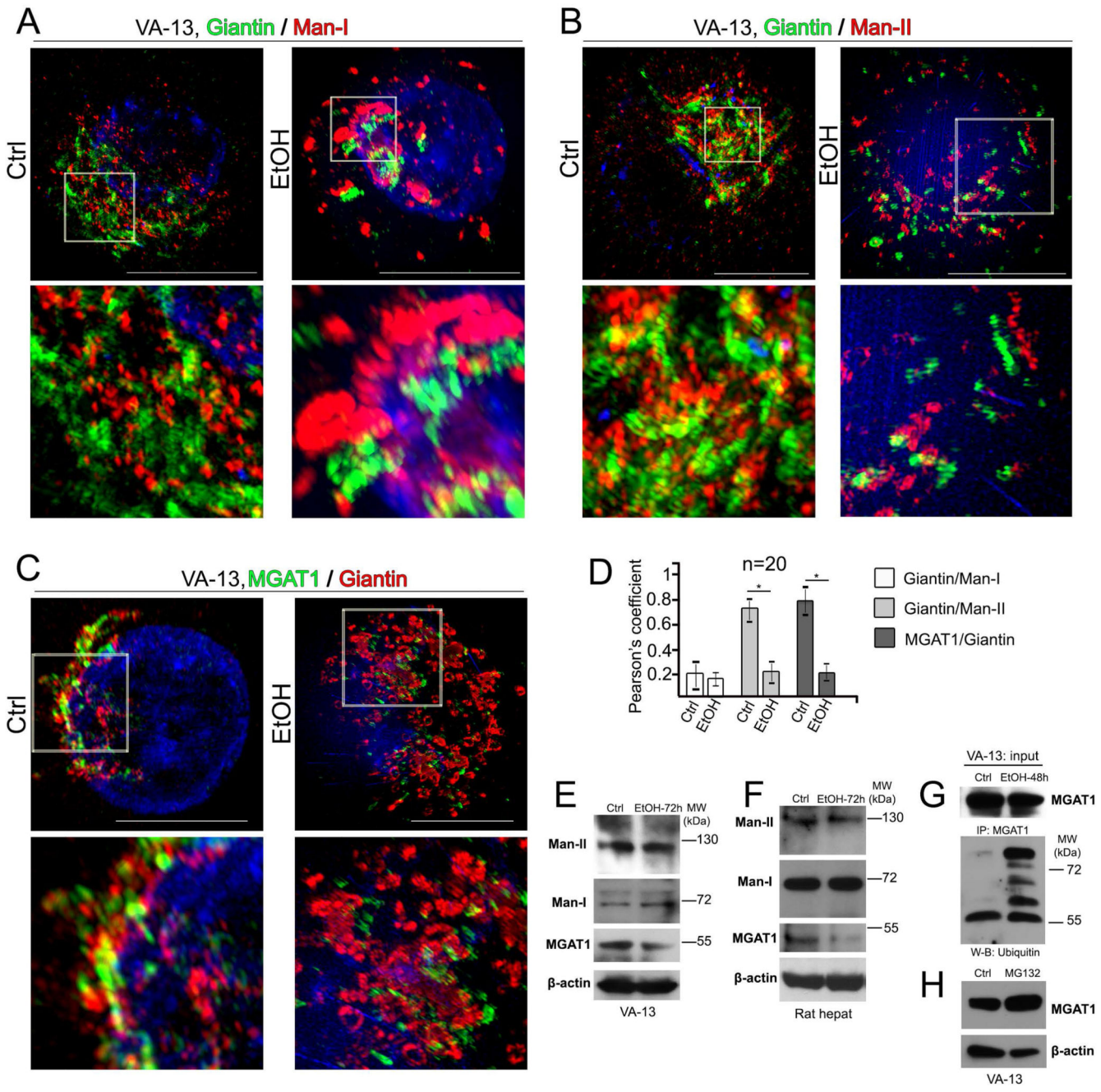

Figure 4.

EtOH treatment reduces the level of MGAT1 and induces redistribution of MGAT1 and Man-II. (A-C) Representative 3D SIM imaging of VA-13 cells before and after treatment with 35 mM EtOH for 72 h. Cells were co-stained with giantin and Man-I (A), giantin and Man-II (B), and MGAT1 and giantin (C). The Golgi area in the white box is enlarged and presented below. Nuclei were counterstained with DAPI (blue). All confocal images were acquired with the same imaging parameters; bars, 10 μm. (D) Quantification of Pearson's coefficient in cells presented in A-C, respectively; n = 20 cells for each series of experiments; results are expressed as a mean ± SD; *, $p<0.001$. (E, F) Man-II, Man-I and

Author Manuscript Author Manuscript Author Manuscript Author Manuscript

MGAT1 Western blot of the lysates of control VA-13 cells and treated with 35 mM EtOH for 72 h (E), and hepatocytes from pair-fed and EtOH-fed rats (F). (G) Ubiquitin western blot of complexes pulled down with anti-MGAT1 Ab from the lysate of VA-13 cells: control or treated with 35 mM EtOH for 48 h. Input was normalized by total protein amount. (H) Western blot of MGAT1 in the lysates of VA-13 cells treated with DMSO (Ctrl) and MG132 (5 μM, 18 h).

Author Manuscript Author Manuscript Author Manuscript Author Manuscript

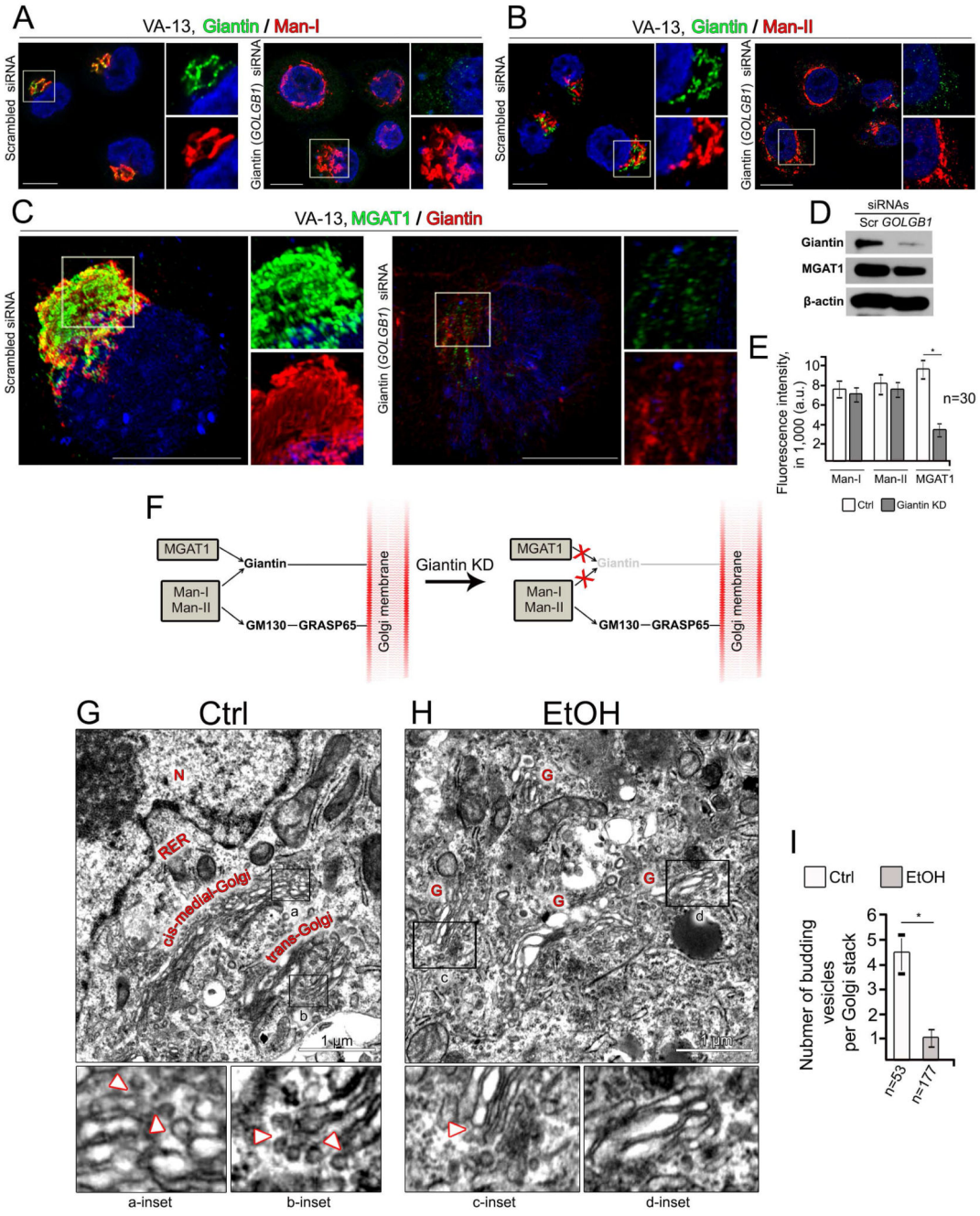

Figure 5.

Differential Golgi targeting mechanism for Man-I, Man-II and MGAT1. (A, B) Immunostaining of giantin and Man-I (A), and giantin and Man-II (B) in VA-13 cells treated with control and giantin siRNAs. (C) Representative 3D SIM imaging of VA-13 cells treated with control and giantin siRNAs. Cells were co-stained with MGAT1 and giantin. The right panels show high magnifications of green and red channels corresponding to the Golgi region (boxes). Nuclei were counterstained with DAPI (blue). All confocal images were acquired with the same imaging parameters; bars, 10 μm. (D) Giantin and MGAT1 Western

Author Manuscript Author Manuscript Author Manuscript Author Manuscript

blot of the lysates of VA-13 cells treated with control or giantin siRNAs; β-actin was a loading control. (E) Quantification of the fluorescence intensity for indicated enzymes in cells presented in A-C. The average fluorescence intensity was measured as a mean ± SD of integrated fluorescence intensity (in arbitrary units, a.u.); n = 30 cells for each series of experiments; *, $p<0.001$. (F) Schema showing Golgi docking mechanism for MGAT1, Man-I and Man-II. Giantin is required for Golgi targeting of MGAT1, and giantin KD (pale colored) blocks MGAT1 trafficking. In the absence of giantin, both Man-I and Man-II are still able to target Golgi through GM130-GRASP65, an alternative docking site. (G-I) EtOH treatment results in reduction of vesicles budding from the Golgi rims. Representative EM micrographs of VA-13 cells: control (G) or treated with 35 mM ethanol for 72 h (H). Black boxes indicate areas enlarged and shown below: a and b are the *cis-medial-* and *trans*-Golgi rims, respectively, from control cell; c and d are the Golgi fragments of EtOH-treated cell. White arrowheads indicate vesicles budding from the Golgi rims. G, Golgi; N, nucleus; RER, rough endoplasmic reticulum. (I) Quantitation summarizing the average number of budding vesicles per Golgi stack. The results from three independent experiments are expressed as a mean ± SD; n, the number of Golgi cisternae for which vesicles were counted; *, $p<0.001$.

Author Manuscript Author Manuscript Author Manuscript Author Manuscript

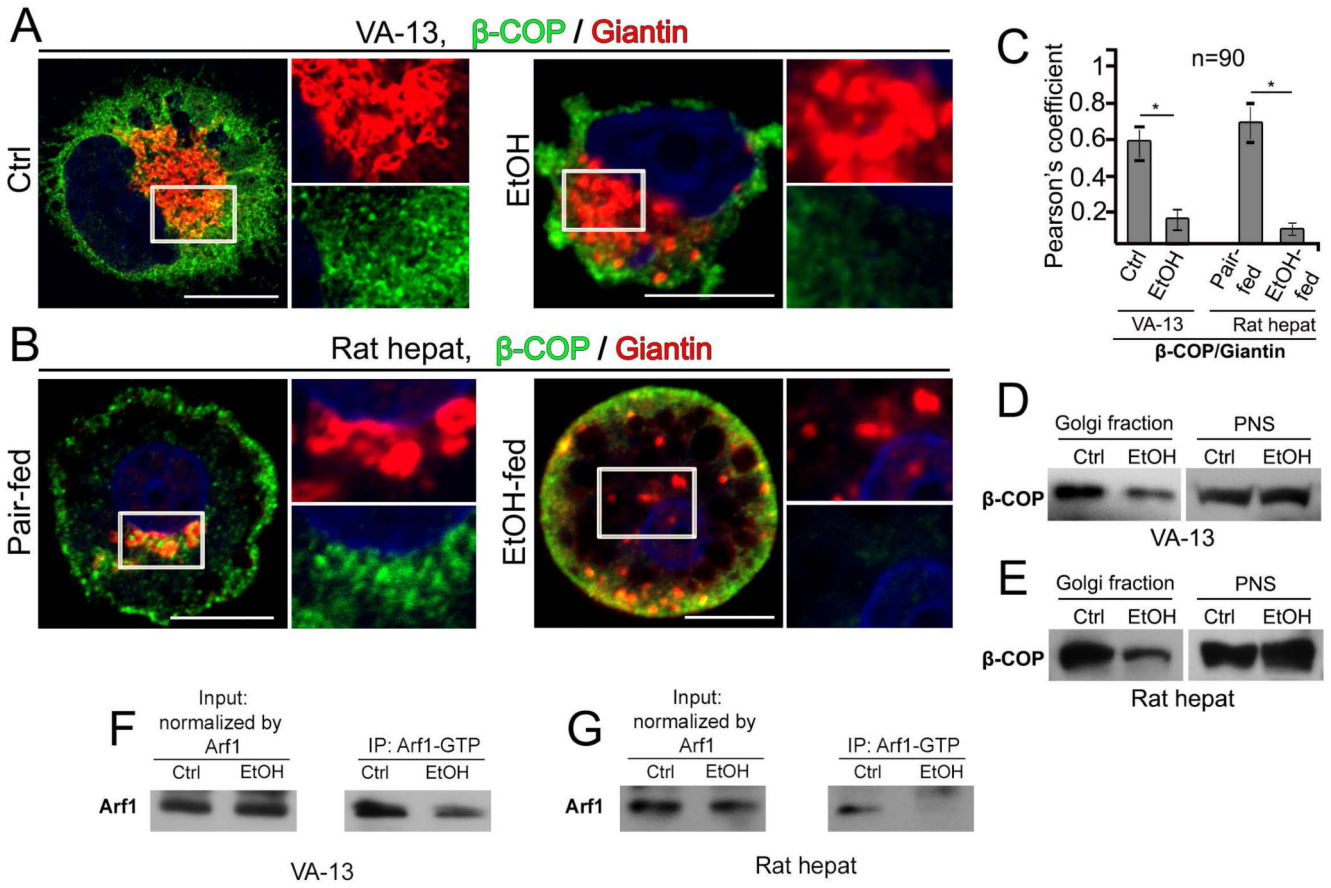

Figure 6.

EtOH treatment reduces COPI and its distribution in the Golgi of VA-13 cells and rat hepatocytes. (A, B) Immunostaining of β-COP and giantin in VA-13 cells (A): no treatment (Ctrl) and EtOH treatment (35 mM) for 72 h, and rat hepatocytes (B): pair-fed and EtOH-fed. The right panels show high magnifications of green and red channels corresponding to the Golgi region (boxes). Nuclei were counterstained with DAPI (blue). All confocal images were acquired with the same imaging parameters; bars, 10 μm. (C) Quantification of Pearson's coefficient between β-COP and giantin in cells presented in A and B, respectively; n = 90 cells from three independent experiments. Results are expressed as a mean ± SD; *, $p<0.001$. (D, E) Western blot of Golgi fractions from the VA-13 cells (D) and rat hepatocytes (E). Golgi membranes were isolated from cells as described in Materials and Methods; 20 μg of Golgi membranes and 35 μg of postnuclear supernatant (PNS) from VA-13 cells, and 15 μg of Golgi membranes and 25 μg of PNS from rat hepatocytes were analyzed for β-COP. Both Golgi and PNS samples were normalized by the total protein amount. (F, G) Arf11 Western blot of the GGA3 PBD agarose beads-Arf1-GTP complexes pulled down from the lysate of VA-13 cells (F) and rat hepatocytes (G) as described in Materials and Methods. The input protein was normalized by total Arf1.

Author Manuscript Author Manuscript Author Manuscript Author Manuscript

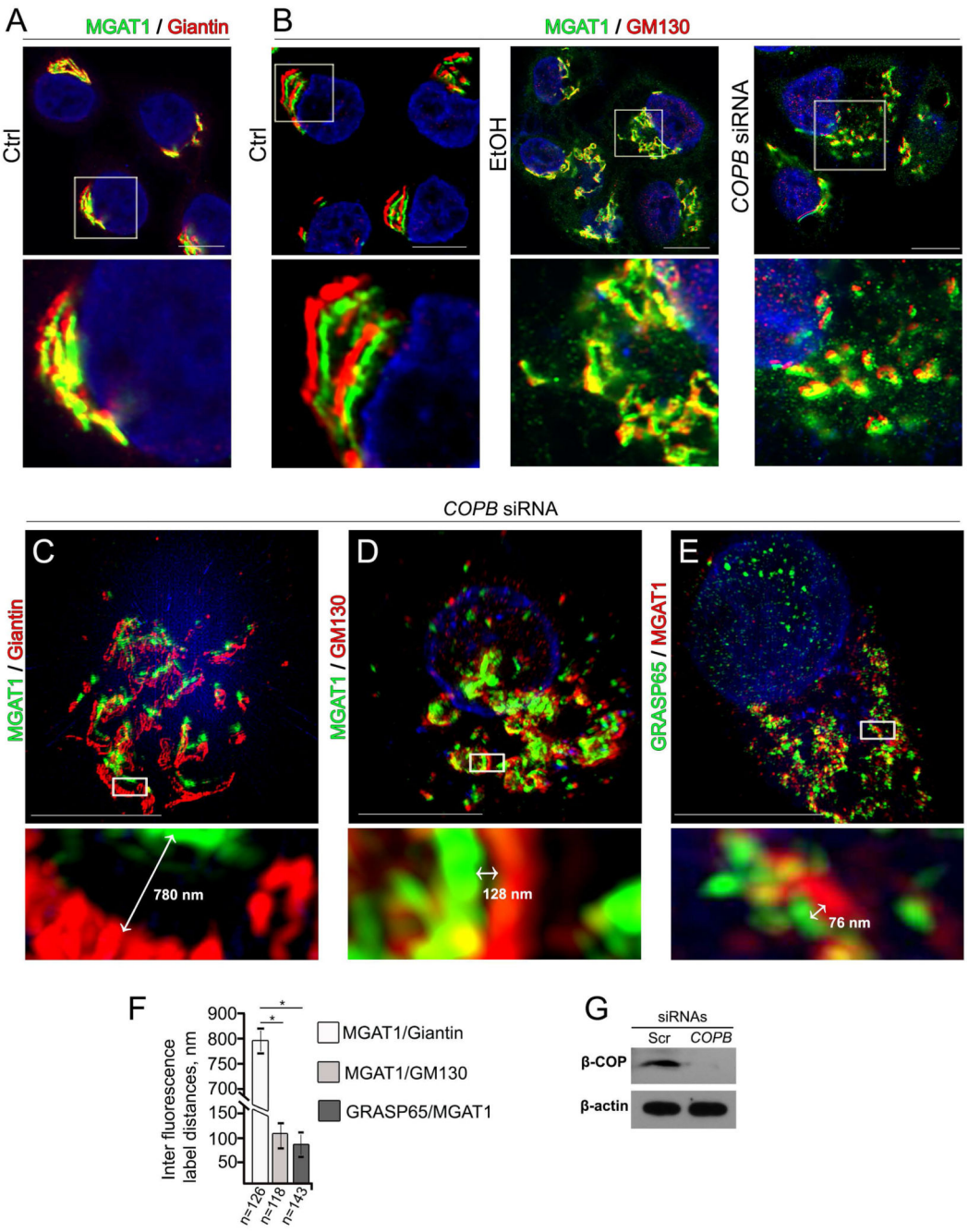

Figure 7.

Treatment with EtOH or KD of β-COP induces redistribution of MGAT1 to the *cis*-Golgi. (A) Immunostaining of MGAT1 and giantin in control VA-13 cells. (B) Immunostaining of MGAT1 and GM130 in control VA-13 cells and VA-13 cells treated with 35 mM EtOH for 72 h, or β-COP siRNAs. The Golgi area in the white box is enlarged and presented below. Nuclei were counterstained with DAPI (blue). All confocal images were acquired with the same imaging parameters; bars, 10 μm. (C-E) Representative 3D SIM imaging of VA-13 cells treated with β-COP siRNAs. Cells were co-stained with MGAT1 and giantin (C),

Author Manuscript Author Manuscript Author Manuscript Author Manuscript

MGAT1 and GM130 (D), and GRASP65 and MGAT1 (E). The Golgi areas with representative inter fluorescence label distance were enlarged and highlighted below (white boxes). (F) Quantification of average green↔red distance in cells presented in C-E. Calculations are performed by ImageJ software as described in Material and Methods and the results are expressed as a mean ± SD, *, $p<0.001$; n - the number of Golgi cisternae for which distance were measured. (G) β-COP Western blot of the lysates of VA-13 cells treated with control or β-COP siRNAs; β-actin was a loading control.

Author Manuscript
Author Manuscript
Author Manuscript
Author Manuscript

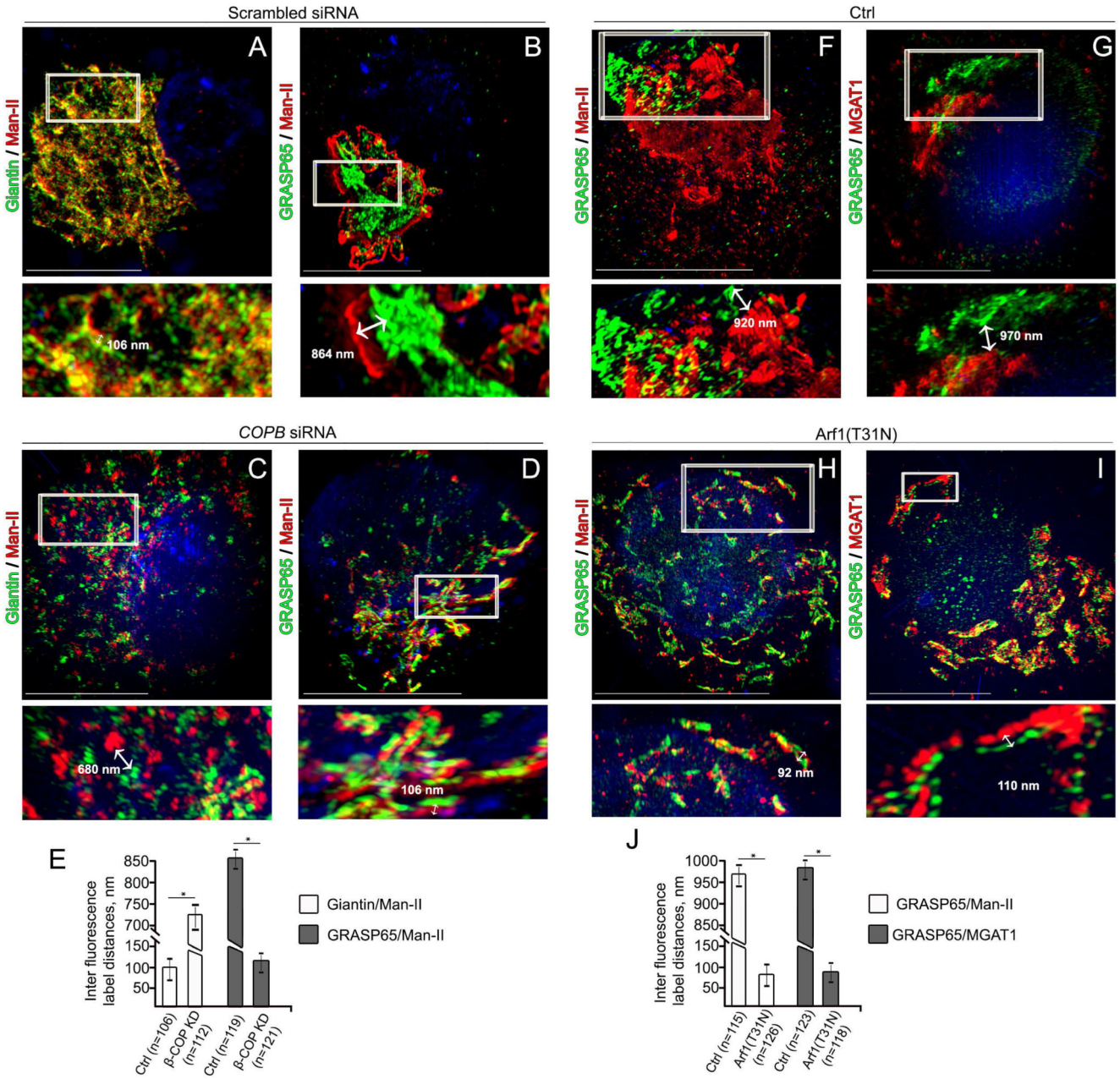

Figure 8.

Treatment with Arf1(T31N) mimics the effect of either EtOH or β-COP KD. (A-D) Representative 3D SIM imaging of VA-13 cells treated with control (A and B) siRNAs, and β-COP siRNAs (C and D). Cells were co-stained with giantin and Man-II or GRASP65 and Man-II, respectively. (E) Quantification of average green↔red distance in cells presented in A-D. (F-I) Representative 3D SIM imaging of VA-13 cells transfected with empty pcDNA3.1 vector (F and G) or Arf1(T31N) plasmid (H and I). Cells were co-stained with GRASP65 and Man-II or GRASP65 and MGAT1, respectively. The Golgi areas with representative inter fluorescence label distance were enlarged and highlighted below (white

Author Manuscript Author Manuscript Author Manuscript Author Manuscript

boxes). (J) Quantification of average green↔red distance in cells presented in F-I. Results are expressed as a mean ± SD, *, $p<0.001$; n - the number of Golgi cisternae for which distance were measured.

Author Manuscript Author Manuscript Author Manuscript Author Manuscript

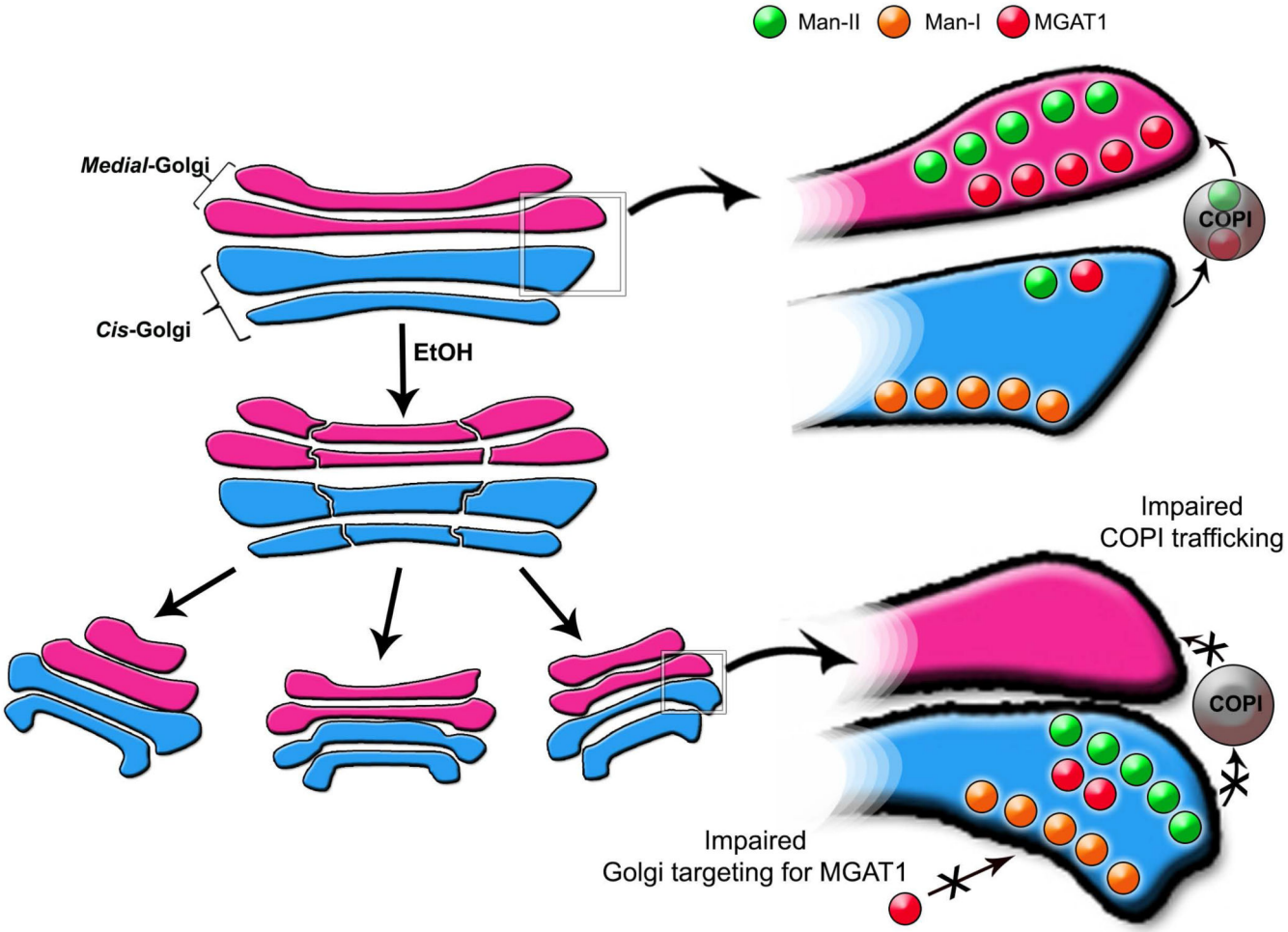

Figure 9.

The proposed model of EtOH-induced alteration in N-glycosylation. Under normal conditions, COPI vesicles regulate distribution of Golgi enzymes: Man-I is in *cis*-Golgi, whereas Man-II and MGAT1 are in *medial*-Golgi (top and right panel). EtOH treatment prevents giantin dimerization, thus disturbing Golgi morphology (Petrosyan et al., 2015a). Golgi undergoes disorganization, which is mediated by a non-muscle Myosin IIA motor protein. In spite of disassembly, Golgi fragments still preserve stacking. However, impaired COPI results in retention of Man-II and MGAT1 in *cis*-Golgi (lower and left panel). In addition, EtOH treatment prevents Golgi targeting of MGAT1 due to alteration of its targeting site.